Molecular Modeling of Methane Diffusion in Glassy Atactic Polypropylene via Multidimensional Transition State Theory

Michael L. Greenfield‡

Department of Chemical Engineering, University of California, Berkeley, Berkeley, California 94720

Doros N. Theodorou*

Department of Chemical Engineering, University of Patras and ICE/HT-FORTH, P.O. Box 1414, GR 26500 Patras, Greece

Received May 11, 1998

ABSTRACT: A multidimensional transition state theory (TST) approach is formulated for the study of elementary jumps involved in the diffusion of a gaseous penetrant in a glassy polymer, taking explicitly into account the coupling between polymer and penetrant degrees of freedom along each jump. In this approach, an initial picture of states (local minima of the potential energy of the polymer + penetrant system) and "macrostates" (i.e., collections of states communicating over barriers small relative to k_BT) is obtained through geometric analysis of accessible volume in representative glassy polymer configurations. Saddle points of the potential energy are computed using the "necks" between accessible volume clusters as initial guesses and progressively augmenting the set of degrees of freedom with respect to which the saddle point is calculated. Starting from the saddle points, states and reaction paths are then mapped out in the multidimensional space of penetrant and polymer degrees of freedom, using Fukui's intrinsic reaction coordinate (IRC) approach, cast in a subset of flexible generalized coordinates. Finally, rate constants for the interstate transitions are computed by multidimensional TST, after invoking a harmonic approximation. Application of this approach to methane at low concentration in glassy atactic polypropylene at 233 K gives well-converged reaction paths involving ca. 350 degrees of freedom of the polymer and confirms the macrostate hypothesis. The rate constant distribution for intermacrostate jumps is found to be very broad, ranging between 10^{-12} and 10^{6} μs^{-1}. The jump length distribution for jumps between states belonging to different macrostates is fairly narrow and centered about 5 Å, which is comparable to the range of motion of the penetrant within a macrostate. Energy barriers for intermacrostate jumps exhibit a broad, asymmetric distribution with mean around 5 kcal/mol, while entropy barriers are much more narrowly and symmetrically distributed with mean around $-4k_B$. The detailed information on elementary jumps gathered by these atomistic TST calculations can form the basis for a coarse-grained model of diffusion and for estimating the diffusivity.

Introduction

The diffusion of small molecules within polymers plays a significant role in many important products and processes. Gas permeation through polymeric films provides clear examples of both barrier property requirements and tailored selectivity needs. Migration of additives within bulk plastics can weaken or eliminate their desired effects. A fundamental understanding of the underlying diffusion processes would help in designing improvements to these complicated systems such that their diffusion properties were better controlled.

Theoretical descriptions of small-molecule diffusion in polymers fall in several categories. In simple molecular theories,[1−6] a particular mechanism for the penetrant motion is invoked and the associated energetics is calculated, leading to estimates of the activation energy and of the diffusion coefficient. In the free-volume approaches,[7−11] the concentration dependence of the penetrant diffusivity is described, starting from a consideration of the average spaces between chains. In the dual-mode transport approach,[12−14] two types of states are postulated and different values are assigned to the four interstate diffusivities. These approaches are described in detail in recent books.[15,16]

All these approaches suffer drawbacks on the molecular level, due to the approximations they invoke to arrive at a closed-form solution. Over the last 10 years, computer simulation has become a common approach for studying the diffusion of individual molecules in melt and glassy polymers. Both molecular dynamics and transition state theory methods have been used. In this paper, we discuss a new methodology for studying infrequent penetrant jump motions within a glassy polymer using highly multidimensional transition state theory. Our approach differs from previous transition state theory-based approaches in including polymer chain motions explicitly along the jump path, thus avoiding artificial, ill-defined parameters. Some results from our work with this approach have already appeared.[17]

Early molecular dynamics (MD) simulations of gas diffusion focused on chemically "simple" polymers, such as polyethylene,[18−26] rubber networks,[27] atactic polypropylene,[28] and polyisobutylene.[25,26,29,30] More recent works have continued those efforts[31−35] and have also considered more chemically "complicated" polymers, such as poly(dimethylsiloxane),[31,36,37] *cis*-polybutadiene,[38] polycarbonate,[39] various polyimides,[40,41] and polystyrene.[42] Similar studies have investigated the diffusion of benzene,[43,44] water,[45,46] and a nifedipine analog[47] in lipid bilayer membranes and of larger molecules in a variety of polymers.[37] Two reviews of small molecule

‡ Present address: Ford Research Laboratory, Ford Motor Co., P.O. Box 2053, Mail Drop 3083/SRL, Dearborn, MI 48121-2053.
* To whom correspondence should be addressed.

S0024-9297(98)00750-5 CCC: $15.00
Published on Web 10/06/1998

diffusion in amorphous polymers have also appeared recently.[39,48]

In most MD investigations, the simulation box contained a small number of penetrants (but more than one) and a single polymer chain, with periodic boundary conditions used to create a "bulk" picture in which the chain interacts with images of itself. After generating trajectories of order nanoseconds, penetrant diffusion coefficients were extracted by applying the Einstein relation to the mean-square penetrant displacement, averaging over all penetrants and multiple time origins.

The success of the MD method relies on diffusion occurring sufficiently quickly. For some gases in some polymers,[26,28,29,31,32,35−38,41,42] the predicted diffusivity was within 1 order of magnitude of the experimental diffusivity. In other cases,[18−25,33,34,37,40] the predicted and measured diffusivities did not agree. It was concluded in some studies[29,49] that polymer structures based on united-atom models led to incorrect diffusivities, while polymer structures based on more detailed models (explicit atoms or anisotropic united atoms) led to diffusivities within 1 order of magnitude of experimental values.

The diffusion mechanism at temperatures below and slightly above the glass transition has been clarified by MD simulations: channels between the penetrant and other sorption sites are briefly opened by small fluctuations in polymer configuration. The penetrant then moves (or hops) through such a channel while it is open, as shown by Takeuchi,[19] Sok et al.,[36] and Müller-Plathe et al.[50] for oxygen in polyethylene, methane in PDMS, and oxygen in PIB, respectively. Greenfield and Theodorou observed similar channel formations in atactic polypropylene without any penetrant present.[51] At temperatures near the glass transition, the frequency of penetrant hops was of order ns^{-1} in a number of simulations: Takeuchi[19] observed the jump mechanism described above but did not observe enough jumps to estimate a diffusivity, Smit et al.[40] observed jumps but were unable to reproduce the experimental diffusivity, and Zhang and Mattice[41] observed jumps and predicted a reasonable diffusivity a few degrees below the glass transition. Since these jumps are rare events in a glassy polymer well below the glass transition, brute force MD cannot sample them properly; most of the simulation time is consumed in tracking fast rattling motions within sorption sites, and jumps are rarely seen. This separation of time scales between rattling and hopping suggests a need for more coarse-grained approaches for simulating penetrant diffusion. Nonequilibrium molecular dynamics (NEMD) has been applied unsuccessfully to diffusion in polyisobutylene;[52] an external field applied within the linear response regime had no effect on the flux (during a reasonable simulation time). Mutual diffusivities were simulated with NEMD in a system of hard-sphere penetrants in a hard-chain polymer,[53] but extracting conclusions about diffusion in a glass or melt from such a system is not straightforward. Sampling of the free energy barrier for water through a lipid bilayer led to order-of-magnitude agreement with experimental results for a system in which diffusion is too slow to simulate directly with MD.[45,46] However, such methods have not been applied to diffusion through a glassy polymer system.

Transition state theory (TST) provides a more approximate treatment of the penetrant diffusion process than MD. Attention is focused on the jumps themselves, and all nonjump motions are integrated over or ignored, yielding the rate at which a penetrant jumps from one region of the simulation cell to another.[54] Transition state theory was first used to simulate diffusion in glassy polymers by Jagodic et al.[56] They could not generate a realistic polymer structure or attain correct potential energy barriers, due to the limited computational resources available at the time. Suter and coworkers have contributed a very substantial body of work using transition state theory to study small penetrant hopping motions in both glassy and melt polymers. Sorption sites were identified as local minima in the three-dimensional potential energy hypersurface imposed on the penetrant by the polymer, rate constants were calculated for inter-site jumps, and kinetic Monte Carlo was used to extract the penetrant diffusivity by tracking a continuous-time−discrete-space random walk between sites. Arizzi[57] considered helium, oxygen, and nitrogen diffusion between tetrahedral interstices in static and fluctuating structures of atactic polypropylene and glassy Bisphenol A polycarbonate. In static structures, he used two different expressions for the rate constant. Using a specified prefactor, the predicted diffusivity was 2 orders of magnitude too high. In fluctuating structures and in static structures with a prefactor determined by a harmonic approximation, the predicted diffusivity was closer to the experimental value. Gusev et al.[39,58−60] simulated penetrant diffusion through glassy and melt polyisobutylene and polycarbonate. First,[58] they assumed that the polymer was static, finding high energy barriers between sorption sites and predicting diffusivities much smaller than 10^{-12} cm^2 s^{-1} for gases other than helium. Next, they considered penetrant diffusion in a polymer whose atoms vibrated harmonically and independently about their equilibrium positions,[59] corresponding to diffusion on an approximate three-dimensional free energy hypersurface. The amplitude of the position fluctuations was a parameter extracted from short-time MD simulations. For the systems under consideration, the predicted and experimental diffusivities agreed within 1 order of magnitude. However, the amplitude of harmonic vibrations was essentially an adjustable parameter, and the sensitivity of the diffusion coefficient to that parameter was not clear; a self-consistent method of evaluating it[59] was later found not to apply in all penetrant−polymer systems.[39] Although computationally economical, the Gusev et al. TST approach disregards direct couplings between polymer and penetrant motions and concomitant polymer relaxations, both of which may be important for larger penetrants, such as alkanes and aromatics. Both their implementations used three-dimensional transition state theory, with the polymer degrees of freedom remaining constant or contributing to an elastic free energy felt by the penetrant. Gray-Weale et al.[61] used approximate contributions to the penetrant−polymer and polymer−polymer potential energy to develop a TST-based model for the penetrant diffusion coefficient. Some predicted trends were in agreement with experimental data.

Directly including polymer contributions to the TST rate constant requires a sufficiently general strategy for determining the jump pathway. Such methods for determining transition state structures and reaction paths may be divided into two broad categories: search-based and path-based. In the search-based (or barrier-

based) methods,[62,63] one searches for a saddle point and then traces the paths through it to the associated local minima. Methods for following the intrinsic reaction coordinate[64] (IRC) typically generate steepest descent trajectories along the gradient (although more elaborate treatments[65−67] have appeared) and have been discussed by Schlegel,[68] in conjunction with transition state search methods. In path-based methods, one begins with pairs of local minima and searches for the path(s) that connect(s) them in configuration space. Pratt formulated a Monte Carlo method for sampling in the transition state region and along the reaction coordinate.[69] The probability of observing a particular path was built up from the probabilities of individual step sequences, assuming a Markov description for the motion between points. Similar methods were implemented by Czerminski and Elber,[70] Gillilan and Wilson,[71] Sevick et al.,[72] Schenter et al.,[73] and Zimmer.[74] In general, these methods are difficult computationally for many points along a multidimensional path; for example, Sevick et al. found that the multidimensional minimization, used to determine the IRC, required evaluation of the Hessian matrix at each state point, an expensive calculation for many degrees of freedom. A transition rate constant may be calculated from structures generated with any of these methods.

For highly multidimensional systems, some investigators have chosen to focus on a limited subset of the system's degrees of freedom. Bulatov and Argon developed a technique for a two-dimensional system of Lennard-Jones spheres in which rows and columns were excised from the Hessian matrix at a transition state, such that the remaining submatrix retained a single negative eigenvalue.[75] Each diffusive jump-type transition thus included a flexible sphere (atom) jumping within an external field imposed by the atoms whose contributions had been removed. For a single-atom jump, they found that all other atoms' contributions could be removed in this manner, and the resulting Hessian retained exactly one negative eigenvalue. However, the displacement of those atoms from their equilibrium configuration was important—it reduced the activation barrier by about 13%. Their technique does not allow a subset of degrees of freedom to be chosen a priori at a transition state or along a reaction coordinate; the entire Hessian must be calculated at the beginning of the procedure. Paulaitis and co-workers used a concept of "essential" degrees of freedom to study dipeptide conformation transitions[76] and polystyrene ring flips.[77,78] They considered either all torsion angles[76] or the backbone−pendant and immediately neighboring backbone−backbone torsion angles (three in all)[77,78] to be flexible along the IRC. After each step in these angles, the potential energy was minimized with respect to bond lengths, bond angles, and (for the polystyrene ring flips) all other torsion angles. Lazaridis et al. presented heuristic arguments as to why this methodology would not affect the location of transition states or the actual minimum energy pathways followed.[76] For some ring flips, however, there was significant correlation between the monitored changes in flexible torsion angles and the induced changes in adiabatically relaxed torsion angles.[78] We will describe a different procedure below for reducing the number of flexible degrees of freedom. In particular, we retain those generalized coordinates defined by atoms that interact directly with the penetrant during the jump. We show that the energy profile reaches an asymptotic limit as the size of this sphere of influence increases.

The objective of this paper is to use computer simulation to determine and analyze the distribution of elementary jumps responsible for diffusion of a gas in a glassy amorphous polymer. Methane in glassy atactic polypropylene is used as a test case, in the limit of small methane concentrations. A methane penetrant molecule was added to pure polypropylene microstructures similar to those whose void distributions were studied in ref 51. The jump rates among accessible sites in each polymer structure were then calculated with methods that are presented here: geometric analysis yielded the necks (or passage points) between pairs of adjacent sorption states, and these points served as initial guesses for transition state locations of the penetrant; multidimensional transition states and diffusion paths were then determined in a subset of all penetrant and polymer degrees of freedom; finally, the rate constant was calculated by invoking a harmonic approximation for the system potential energy at the sorption state minima and transition state saddle points. In summary, we coupled a very good initial-guess strategy for the transition state position of the penetrant with a direct saddle-point search technique. Sequences of steps along the IRC were used to connect saddle points with their associated local minima. The simulation results are based on 208 diffusion paths in six independent polymer structures. Each initial polymer structure is in detailed mechanical equilibrium; the net force on all atoms equals zero. Though we only describe methane in glassy atactic polypropylene, these methods are sufficiently general that they could be used to simulate diffusion of any flexible penetrant in any host material, as long as the diffusion mechanism retained a jumplike character.

This paper is devoted to considering single penetrant jump properties. The transition state structure, jump rate and jump length distributions, and polymer contributions to the penetrant jump process will be discussed, without incorporating correlations between consecutive jumps. We begin with equations for the transition state location, intrinsic reaction coordinate (IRC), and rate constant in the full dimensionality, within a generalized coordinate system. Next, we derive expressions for the transition state and diffusion path that encompass changes in only a flexible subset of the total number of generalized coordinates. The remaining degrees of freedom remain flexible conceptually but are bound to their equilibrium positions by infinitely stiff springs. Then we derive formulas for the penetrant jump rate constants, approximating the potential energy harmonically in the vicinity of a transition state or a local minimum, and discuss how the derived methodologies were implemented.

Formulation of Multidimensional TST in Generalized Coordinates

TST is a classical methodology for treating infrequent event processes that involve crossing a barrier significantly higher than the thermal energy $k_B T$.[55] The complicated dynamical paths followed by an N-body system are reduced to a statistical description, and sampling is performed over local fluctuations in order to answer the question, "How much time goes by (on average) before the system resides in a definably different portion of configuration space?" Phenomenologi-

cally, a set of first-order rate constants describe the rate of evolution along different available pathways.[79] Transition state theory provides a means to calculate such rate constants by comparing the probability of the system lying on a dividing surface, which separates two states, to the probability of occupying an initial state.

Applying transition state theory involves a number of linked steps: locating stable regions in configuration space, identifying transition states and dividing surfaces between the stable regions, following pathways along which the system passes from stable region to stable region, and calculating the rate of the entire process. These aspects are derived here for penetrant jump motions in a glassy polymer. Stable regions for the penetrant to occupy in the glassy polymer were determined prior to the search for transition states, using methods from ref 51.

The basis of the polypropylene model was described in ref 80. Explicit C and H atoms and united-atom CH_3 groups comprise the $N_c = 3$ monodisperse polypropylene chains of $n_{un} = 50$ monomer units, with $6n_{un} - 1$ atoms and groups on each. The single methane penetrant is treated as a united-atom sphere. The total potential energy includes contributions from a four-body torsional potential,

$$V^{\phi} = \sum_i \frac{1}{2} k_{\phi}(1 - \cos 3\phi_i) \tag{1}$$

a three-body bond angle potential,

$$V^{\theta} = \sum_i k_{\theta}(\theta_i - \theta_{i_0})^2 \tag{2}$$

and two-body nonbonded interactions among different groups on the polymer chains and between the penetrant and each group on the chains. Polymer−polymer interactions were described with the Slater−Kirkwood potential for each group−group interaction,

$$\epsilon_{ij} = \frac{1}{4}\frac{{c_{ij}}^2}{a_{ij}}$$
$$\sigma_{ij} = \left(\frac{a_{ij}}{c_{ij}}\right)^{1/6} = 2^{-1/6}(r_{\mathrm{vdW}_i} + r_{\mathrm{vdW}_j}) \tag{3}$$

where

$$c_{ij} = \frac{3}{2}\frac{e\hbar}{{m_e}^{1/2}}\frac{\alpha_i\alpha_j}{(4\pi\epsilon_0)^2}\left(\left(\frac{\alpha_i}{n_{e_i}}\right)^{1/2} + \left(\frac{\alpha_j}{n_{e_j}}\right)^{1/2}\right)^{-1}$$

is a function of the polarizability α and effective number of electrons n_e and

$$a_{ij} = \frac{1}{2}c_{ij}(r_{\mathrm{vdW}_i} + r_{\mathrm{vdW}_j})^6$$

is determined by requiring that the pairwise intermolecular force equals zero at the sum of the van der Waals radii $r_{\mathrm{vdW}_i} + r_{\mathrm{vdW}_j}$. Penetrant−polymer interactions were described with a Lennard-Jones potential,

$$V^{\mathrm{LJ}} = 4\epsilon_{ip}\left[\left(\frac{\sigma_{ip}}{r_{ip}}\right)^{12} - \left(\frac{\sigma_{ip}}{r_{ip}}\right)^{6}\right] \tag{4}$$

using penetrant−atom interaction parameters determined from

$$\epsilon_{ip} = \sqrt{\epsilon_{ii}\epsilon_{pp}} \qquad \sigma_{ip} = (\sigma_{ii} + \sigma_{pp})/2$$

Pure-species parameters were obtained from ref 81 for methane and from eq 3 (via ref 80) for the polymer constituents. The three chains and single penetrant were folded into a three-dimensional cube with edge length 22.79 Å, corresponding to the experimental atactic polypropylene density 0.892 g/cm^3 at 233 K and initial sorption with no change in volume. (Ignoring dilation is reasonable at low concentration since the partial molar volume of a gas is significantly lower in a glassy polymer than in a polymer melt or in an organic liquid.[82]) Three-dimensional periodic boundary conditions were used to prevent surface effects.

To prevent the fast vibrations of H−C−H angles,[83] we undertook steps to eliminate the hydrogen atom positions from the equations of motion.[84] To maintain some explicit atom character, the hydrogen atoms of CH_2 and CH−R groups were used as force centers, but their mass was transferred to the skeletal carbon atoms to which they were bound. Their positions were defined explicitly by the positions of the surrounding heavy atoms according to the following rules. For a CH_2 group on segment i, the C_{i-1}−C_i−C_{i+1} and H−C_i−H planes were mutually perpendicular and bisected the H−C_i−H and C_{i-1}−C_i−C_{i+1} angles, respectively; each H−C_i−H angle supplement equaled 73.42°. For a CH group on segment i, the C_i−H bond was perpendicular to the C_{i-1}−R_i−C_{i+1} plane. All C−H bond lengths were 1.1 Å.

A full description of all chain configurations can be provided in terms of the vector of Cartesian coordinates $\mathbf{X} = X^1, X^2, ..., X^{3N}$ of the $N = N_c(3n_{un} + 1)$ heavy atoms and groups. For each atom, the mass-weighted coordinates were obtained from its Cartesian coordinates through multiplication by the square root of its mass:

$$x^i = {m_i}^{1/2}X^i \tag{5}$$

In describing the configuration of the polymer + penetrant system, the vector $\mathbf{x}$ was augmented to include three mass-weighted coordinates of the spherical penetrant, obtained from its three Cartesian coordinates $\mathbf{X}_{pen}$ and its mass m_{pen} through eq 5. Note that, due to the translational periodicity of the model penetrant + polymer system, its potential energy depends on only $3N$ of the $3N + 3$ components of the augmented vector $\mathbf{x}$. In the calculations reported below, one chain start position (that lying furthest from the penetrant) was kept fixed. The symbol $\mathbf{x}$ will be used to denote the $3N$-dimensional vector of mass-weighted Cartesian coordinates of the remaining atoms, including the penetrant.

Polymer configurations residing in local minima of the pure polymer potential energy hypersurface were taken as initial estimates of the polymer configuration at the transition states of penetrant jumps. These structures were generated as in ref 80, with the addition of flexible bond angles. These structures are just initial estimates for the identification of transition states; their use does *not* imply that polymer chains remain frozen during the penetrant diffusion process.

To maintain infinitely stiff degrees of freedom at constant values, we change to a system of generalized

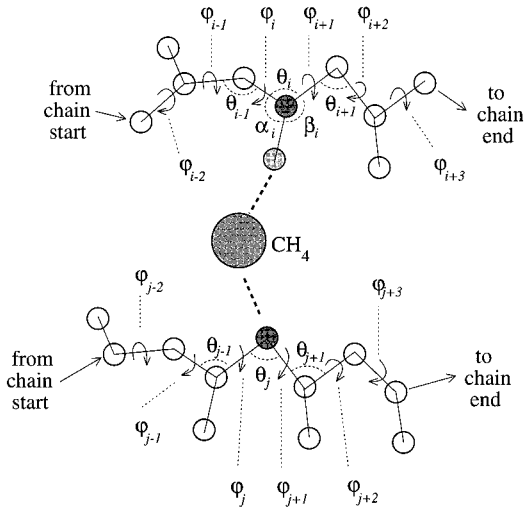

Figure 1. Choice of local, flexible generalized coordinates for a given penetrant−polymer segment interaction. For each segment i neighboring the penetrant, the generalized coordinates (ϕ_{i-2}, ϕ_{i-1}, θ_{i-1}, ϕ_i, θ_i, ϕ_{i+1}, θ_{i+1}, ϕ_{i+2}, ϕ_{i+3}) were selected to be flexible. If the segment was chiral, the generalized coordinates (α_i, β_i) were additionally selected to be flexible. Near the chain start, the start position $\mathbf{x}^{st}$ and the Eulerian angles (ψ_1, ψ_2, ψ_3) were also made flexible; near the chain end, the flexible angles were dropped as they "fell off" the chain. The upper picture depicts the selected coordinates for a chiral segment; the lower picture depicts analogous information for an achiral segment. Atomic radii are shrunk and hydrogen atoms are omitted for clarity.

coordinates for each chain (see also Figure 1): a three-dimensional vector of mass-weighted chain start coordinates, $\mathbf{x}^{st}$; a $3n_{un}$-dimensional vector of C−C and C−CH_3 bond lengths, $\boldsymbol{l}$; a three-dimensional vector of Euler angles, $\boldsymbol{\psi}$; a $2n_{un}-1$-dimensional vector of skeletal C−C−C bond angles, $\boldsymbol{\theta}$; two n_{un}-dimensional vectors of C−C−R bond angles, $\boldsymbol{\alpha}$ and $\boldsymbol{\beta}$; and a $2n_{un}-2$-dimensional vector of skeletal torsion angles, $\boldsymbol{\phi}$. The generalized coordinates ($\mathbf{x}^{st}$, $\boldsymbol{l}$, $\boldsymbol{\psi}$, $\boldsymbol{\theta}$, $\boldsymbol{\phi}$, $\boldsymbol{\alpha}$, $\boldsymbol{\beta}$) for each chain, along with $\mathbf{x}_{pen}$ for the penetrant, are represented generally as $q^i = f^i(x^1, ..., x^{3N})$, $i = 1, 2, ..., 3N$ with unique inverses $x^i = g^i(q^1, ..., q^{3N})$. Potential energy gradients with respect to generalized and to mass-weighted Cartesian coordinates are related by

$$\frac{\partial V}{\partial x^i} = \sum_{j=1}^{3N} \frac{\partial q^j}{\partial x^i} \frac{\partial V}{\partial q^j} \tag{6}$$

and

$$\frac{\partial V}{\partial q^i} = \sum_{j=1}^{3N} \frac{\partial x^j}{\partial q^i} \frac{\partial V}{\partial x^j} \tag{7}$$

while differential changes in position are related by

$$\mathrm{d}x^i = \sum_{j=1}^{3N} \frac{\partial x^i}{\partial q^j} \mathrm{d}q^j \tag{8}$$

and

$$\mathrm{d}q^i = \sum_{j=1}^{3N} \frac{\partial q^i}{\partial x^j} \mathrm{d}x^j \tag{9}$$

These equations can also be expressed in matrix form as

$$\nabla_{\mathbf{x}} V = J^{\mathrm{T}} \nabla_{\mathbf{q}} V \qquad \nabla_{\mathbf{q}} V = (J')^{\mathrm{T}} \nabla_{\mathbf{x}} V \tag{10}$$

$$\mathrm{d}\mathbf{x} = J' \, \mathrm{d}\mathbf{q} \qquad \mathrm{d}\mathbf{q} = J \, \mathrm{d}\mathbf{x} \tag{11}$$

where $\nabla_{\mathbf{x}} V$ and $\nabla_{\mathbf{q}} V$ are column vectors that contain the derivatives of the total potential energy with respect to each mass-weighted Cartesian (x^i) or generalized (q^i) coordinate. The conformation-dependent *matrices* J and J' are calculated as

$$J = \begin{pmatrix} \partial q^1/\partial x^1 & \cdots & \partial q^1/\partial x^{3N} \\ \vdots & & \vdots \\ \partial q^{3N}/\partial x^1 & \cdots & \partial q^{3N}/\partial x^{3N} \end{pmatrix} \tag{12}$$

$$J' = \begin{pmatrix} \partial x^1/\partial q^1 & \cdots & \partial x^1/\partial q^{3N} \\ \vdots & & \vdots \\ \partial x^{3N}/\partial q^1 & \cdots & \partial x^{3N}/\partial p^{3N} \end{pmatrix} \tag{13}$$

and are inverses of each other. The matrix products $\mathbf{a} = J'^{\mathrm{T}} J'$ and $\mathbf{a}^{-1} = J J^{\mathrm{T}}$ define the covariant and contravariant metric tensors, following notation from ref 85.

The transition state is defined as a first-order saddle point on the $3N$-dimensional potential energy hypersurface. Hence, all elements of the potential energy gradient equal zero

$$\frac{\partial V}{\partial X^i} = 0 \tag{14}$$

and all eigenvalues of the Hessian matrix of second derivatives of the potential energy with respect to mass-weighted Cartesian coordinates but one are positive,

$$\mathbf{H}\mathbf{x}'_j = \lambda_j \mathbf{x}'_j \qquad \begin{cases} \lambda_j < 0 & j = 1 \\ \lambda_j > 0 & j = 2, ..., 3N \end{cases} \tag{15}$$

The notation $\mathbf{x}'_j$ in eq 15 indicates the jth eigenvector. The same forms of eq 14 apply in mass-weighted Cartesian coordinates, since

$$\frac{\partial V}{\partial x^i} = \frac{1}{m_i^{1/2}} \frac{\partial V}{\partial X^i} = 0 \tag{16}$$

Likewise, in generalized coordinates, at any stationary point with respect to the mass-weighted Cartesian coordinates, eq 10 becomes a $3N \times 3N$ system of the general form $\mathbf{A}\mathbf{y} = 0$, for which either $\mathbf{y} = \nabla_{\mathbf{q}} V = 0$ or $\det \mathbf{A} = \det J^{\mathrm{T}} = \det J = 0$. Since the $3N$ primary mass-weighted Cartesian coordinates ($\mathbf{x}$) are orthogonal to one another and the $3N$ generalized coordinates ($\mathbf{q}$) span the same space, the Jacobian $\det J$ must be nonzero; hence $\nabla_{\mathbf{q}} V = 0$ at any configuration for which $\nabla_{\mathbf{x}} V = 0$.

A system displaced slightly from a transition state experiences forces that direct it even further away, and the net displacement increases until the system thermalizes in the region surrounding a local minimum. Depending on the direction of the initial displacement, the system will find itself near one of two local minima. These two regions share a common dividing surface, which passes through the transition state. The exact pathway that would be followed between the transition

state and the associated local minima, in the limit of infinitely small displacements and with continuous application of a frictional force equal and opposite to the forces arising from the potential energy gradient, has been termed the intrinsic reaction coordinate (IRC) by Fukui.[64] The term "reaction" refers to the common application of TST to chemical reaction dynamics; here, the IRC refers to the changes in penetrant and polymer degrees of freedom that describe the mechanism of a particular penetrant jumping motion. The IRC is a steepest descent trajectory[86] in mass-weighted Cartesian coordinates, and it corresponds physically to a sequence of infinitesimal displacements along the local force vector. A true system undergoing molecular dynamics would not follow this path exactly; rather, the IRC defines a baseline about which a true system would fluctuate.

Fukui[64] has derived the equation

$$\mathbf{a}\, d\mathbf{q} = \nabla_{\mathbf{q}} V\, d\tau \tag{17}$$

for the step $d\mathbf{q}$ to take along the IRC in generalized coordinates, at any point other than the transition state, with τ a parameter measuring progress along the reaction path. Equation 17 is thus a prescription for following the diffusion path in the full $3N$ generalized coordinates in a system for which the coordinate transformation derivatives $\partial\mathbf{x}/\partial\mathbf{q}$ are convenient to calculate. The prescription calls for calculating the gradient $\nabla_{\mathbf{q}} V$ and the matrix $\mathbf{a}$, solving a series of $3N$ linear equations for the step vector $d\mathbf{q}$, and scaling each term by the same small constant $d\tau$. The elements of J' (and thus the elements of $\mathbf{a}$) will vary with system configuration and must be recalculated after each step. The importance of including the matrix $\mathbf{a}$ has been discussed previously by Banerjee and Adams.[88] This matrix is not diagonal in general, and thus it couples the step along one coordinate dq^i to the gradient with respect to many q^j ($j \neq i$).

The step along the IRC defined by eq 17 is undefined at the transition state, since there the potential energy gradient equals the zero vector. Many investigators[65,89] have stated that the proper step to take in this case is directed along the eigenvector corresponding to the negative eigenvalue of the Hessian matrix (found with respect to mass-weighted Cartesian coordinates). This is the sole direction of decreasing local curvature, and it is orthogonal to all directions of increasing local curvature. This choice for the first step relies implicitly on the use of an orthogonal coordinate system, such as mass-weighted Cartesian coordinates, for which the metric tensor is diagonal. The extension of this formalism to generalized coordinates has been discussed by Banerjee and Adams.[88] First, an equivalent Hessian must be found with respect to the generalized coordinates. Expanding partial derivatives via the chain rule,

$$\mathbf{H} = J^{\mathrm{T}} \mathbf{H}_{qq} J + \left(\frac{\partial^2 \mathbf{q}^{\mathrm{T}}}{\partial x^i \partial x^j}\right) \nabla_{\mathbf{q}} V \tag{18}$$

where $\mathbf{H}_{qq}$ is the Hessian with respect to generalized coordinates, and $\partial^2\mathbf{q}^{\mathrm{T}}/\partial x^i \partial x^j$, a third-rank tensor, may be thought of as a $3N \times 3N$ matrix in which each component, itself a vector, contains the coordinate transformation second derivatives of $\mathbf{q}$ with respect to x^i and x^j. The resulting rightmost term in eq 18 is a matrix for which the ijth element is the dot product of the ijth vector with $\nabla_{\mathbf{q}} V$.

The eigenvectors of $\mathbf{H}$ in the mass-weighted Cartesian coordinate system would be found in the standard way,

$$\mathbf{H}\mathbf{x}' = \lambda \mathbf{x}' \tag{19}$$

Substituting for $\mathbf{H}$ with eq 18 and converting $\mathbf{x}'$ into generalized coordinates with eq 11 leads to

$$\mathbf{H}_{qq}\mathbf{q}' + J'^{\mathrm{T}} \left(\frac{\partial^2 \mathbf{q}^{\mathrm{T}}}{\partial x^i \partial x^i}\right) \nabla_{\mathbf{q}} V\, J' \mathbf{q}' = \lambda \mathbf{a}\mathbf{q}' \tag{20}$$

If we restrict attention to the transition state, where $\nabla_{\mathbf{q}} V = 0$, then we find

$$\mathbf{H}_{qq}\mathbf{q}' = \lambda \mathbf{a}\mathbf{q}' \tag{21}$$

a generalized eigenvalue problem in which $\mathbf{a}$ is positive definite. The units on each side match exactly,

$$(\mathbf{H}_{qq}\mathbf{q}')_i\ [=] \sum_j \frac{\text{energy}}{q_i q_j} q_j = \frac{\text{kg m}^2}{\text{s}^2\, q_i}$$

$$(\mathbf{a}\mathbf{q}')_i\ [=] \sum_j \frac{(\text{kg}^{1/2}\ \text{m})^2}{q_i q_j} q_j = \frac{\text{kg m}^2}{q_i}$$

and λ has units of $1/\text{s}^2$, or frequency squared, as expected. The first step should be taken along the normal mode $\pm\, \mathbf{q}'_1$, with $\lambda_1 < 0$.

Reduction to a Subset of Flexible Coordinates. The development so far has considered the transition state structure and diffusion pathway in generalized coordinates but has remained in the full $3N$ dimensions. The physics of the diffusion process allows the dimensionality to be reduced considerably. The generalized coordinates can be divided into three sets. One set, the bond lengths $\boldsymbol{l}$, are considered flexible in the limit of infinite stiffness (following the nomenclature of Gō and Scheraga[90]); the value of each bond length is assumed to be the same at the local minima and at the transition state. In a sufficiently large penetrant−polymer system, a second set is composed of the many generalized coordinates describing atoms far from the penetrant. If the fluctuation among polymer chains that allows a penetrant to jump is indeed local, the values of this multitude of coordinates should not be appreciably different at the origin state, saddle point, or destination state. Evidence for the local nature of jumps comes from MD simulations. For example, Pant and Boyd[26] found that torsion angles in polyisobutylene, at temperatures slightly above the glass transition, did not lose significant correlation over the time scales on which methane penetrants hopped. In accordance with channel opening having a local nature, we allowed only a third set, those nonconstrained generalized coordinates defined by atoms near the jumping penetrant, to be "flexible" when describing a transition state structure. Both other sets of degrees of freedom were held constrained to their initial values (in the energy-minimized neat polymer structure) by springs whose force constants approached infinity.

In Appendix A we derive appropriate expressions for the transition state location and the first and subse-

quent steps along the IRC in this reduced set of coordinates. We find

$$\frac{\partial V}{\partial q^{\alpha}} = 0 \tag{22}$$

at a transition state with respect to each flexible generalized coordinate q^{α}. The first step away from the transition state is directed along $\pm (\mathbf{q}_f')_1$, found from

$$\mathbf{H}^0_{qq}(\mathbf{q}_f')_i = \lambda_i \mathbf{a}^0 (\mathbf{q}_f')_i \tag{23}$$

where $\mathbf{H}^0_{qq}$ and $\mathbf{a}^0$ are the submatrices of $\mathbf{H}_{qq}$ and $\mathbf{a}$ in which both generalized coordinates appearing in the derivatives are flexible, λ_1 is the sole negative eigenvalue, and $(\mathbf{q}_f')_i$ is the ith eigenvector in the f flexible coordinates. Vibrational frequencies are determined from

$$\nu_i = \lambda_i^{1/2}/2\pi \tag{24}$$

Subsequent steps were taken using

$$\mathbf{a}^0 \, \mathrm{d}\mathbf{q}_f = \nabla_{\mathbf{q}_f} V \, \mathrm{d}\tau \tag{25}$$

where $\mathrm{d}\mathbf{q}_f$ represents the changes in flexible generalized coordinates along the step. The distance traveled along the reaction path during each step is given by eq 43 in Appendix A.

This method could also be applied in a subset of the mass-weighted Cartesian coordinates. It would be necessary to choose an appropriate subset of flexible atoms and either to incorporate flexible bond lengths or to derive an appropriate metric tensor $\mathbf{a}^0$ that preserves infinitely stiff bond lengths along the interface between the flexible and constrained atoms.

Calculation of the Jump Rate Constant. After finding the local minima $\mathbf{q}^{\min}$, the transition state location $\mathbf{q}^{\ddagger}$, and the pathways connecting them (in terms of a subset of flexible generalized coordinates), the next step is to calculate the corresponding first-order rate constant. The general transition state theory expression for the rate constant,

$$k^{\mathrm{TST}} = \frac{k_B T}{h} \frac{Q^{\ddagger}}{Q} = \frac{k_B T}{h} \exp\left(-\frac{\Delta A}{k_B T}\right) \tag{26}$$

requires three different elements: (1) a description of the boundary (dividing surface) between adjacent regions in configuration space, constructed around the state minima; (2) a method of evaluating the partition function Q in the origin state; and (3) a method of evaluating $Q^{\ddagger}$ for the system confined to the multidimensional dividing surface. The integration domain for the partition function along the dividing surface is smaller by one dimension than that of either state region, since integration is limited to the $(3N-1)$-dimensional dividing surface that passes through the transition state. An exact differential equation for this surface is known,[64] but its evaluation is difficult; it amounts to following the $3N-1$ IRCs defined by taking the first step along an eigenvector associated with a positive eigenvalue. In this work, we approximated the dividing surface near the transition state with a hyperplane orthogonal to the eigenvector corresponding to the negative eigenvalue; the dividing plane was orthogonal to the step taken away from the transition state. This surface is a first-order approximate solution to the $3N-1$ differential equations. The dividing surface can thus be written in a flexible subset of generalized coordinates as

$$(\mathbf{q}_f - \mathbf{q}_f^{\ddagger})^{\mathrm{T}} \mathbf{a}_0 \mathbf{q}'_{f_1} = 0 \tag{27}$$

where $\mathbf{q}'_{f_1}$ is the eigenvector that corresponds to the negative eigenvalue in the flexible subset of generalized coordinates.

We calculated the partition functions via a harmonic approximation for the potential energy, performed with respect to the flexible generalized coordinates in a manner that is independent of the coordinate system. Vineyard presented similar results long ago for the harmonically approximated rate in a full set of mass-weighted Cartesian coordinates.[91] In nonorthogonal generalized coordinates, we show in Appendix B that the rate may be expressed as

$$k^{\mathrm{TST}} = \frac{\prod_{\alpha=1}^{f} \nu_{\alpha}}{\prod_{\alpha=2}^{f} \nu_{\alpha}^{\ddagger}} \left[\frac{\det \mathbf{a}^{-1''}}{\det (\mathbf{a}^{-1''})^{\ddagger}}\right]^{1/2} \exp\left[-\frac{(V^{\ddagger} - V_0)}{k_B T}\right] \tag{28}$$

using a classical partition function for each harmonic oscillator, or

$$k^{\mathrm{TST}} = \frac{k_B T}{h} \frac{\prod_{\alpha=1}^{f}\left[1 - \exp\left(-\frac{h\nu_{\alpha}}{k_B T}\right)\right]}{\prod_{\alpha=2}^{f}\left[1 - \exp\left(-\frac{h\nu_{\alpha}^{\ddagger}}{k_B T}\right)\right]} \exp\left[-\frac{(V^{\ddagger} - V_0)}{k_B T}\right] \tag{29}$$

using a quantum-mechanical partition function for each harmonic oscillator. The matrix $\mathbf{a}^{-1''}$ is a submatrix of the contravariant metric tensor, $\mathbf{a}^{-1}$, corresponding to gradients in eq 12 in which all q^i's refer to infinitely stiff generalized coordinates. An explicit expression for $\det \mathbf{a}^{-1''}/\det(\mathbf{a}^{-1''})^{\ddagger}$ is presented in ref 84, using the Fixman relation.[90] The jump rate constants reported here were calculated using eq 29. To our best knowledge, the derivations of Appendix B have not been presented before for the rate in a subset of nonorthogonal generalized coordinates.

Computation of Transition States and Reaction Paths

Finding a transition state between two sorption states via eq 22 requires several iterative steps. After specifying the initial polymer structure, an initial guess must be chosen for the penetrant location at the transition state, and then flexible polymer degrees of freedom must be selected. Our strategy is based on successively augmenting the subspace of flexible degrees of freedom with respect to which the saddle point of the energy is calculated, until all relevant degrees of freedom have been included. This process is analogous to relaxation of the polymer conformation, except that the goal is a first-order saddle point, rather than a local minimum. The search strategy is based on a geometric analysis of the polymer configuration, taken from ref 51. Our initial guess strategy is based on a hypothesis that

polymer chain conformation does not change significantly in a glassy polymer over long time scales. NMR studies[92] of glassy atactic polypropylene support this view, showing that times greater than 1 s are required for backbone conformations to decorrelate. Consequently, the atomic-level voids (defined by clusters of accessible volume) that exist at some initial time are likely to continue to exist over time scales longer than those of penetrant diffusion. The initial guess procedure was designed to find these voids in particular polymer conformations and then to utilize spherical (hypothetical penetrant) probes of reduced diameter to locate where intervoid channels could open.

The initial estimate of the penetrant position at the transition state was determined with the geometric analysis method developed in ref 51. First, the three-dimensional simulation box was divided into Delaunay tetrahedra, and lists of tetrahedra accessible to different hard-sphere probes were determined. For a "large" sized probe radius, $r_p = 1.28$ Å, accessible regions were found to be separated from one another, and each distinct hole (or void) was given an identity label: 1, 2, ..., N_{voids}. For a smaller hypothetical probe radius, $r_p = 0.63$ Å, newly accessible pathways connected the original voids. Within this picture, the pathways (accessible to the small probe) that existed between voids (accessible to both large and small probes) defined a set of tetrahedra that spanned the region between the voids. Using the connectivity algorithm described in ref 51, each tetrahedron was labeled with the identity of the original void to which it first became connected as the probe radius decreased. Within this set of tetrahedra are certain ones whose "identity" differs from the labeled identity of one to three (of their four) tetrahedral neighbors. Such pairs (the tetrahedron and its neighbor with a different identity) denote intersections, at which the pathways emanating from two voids join together. The geometric centroids

$$\mathbf{X}_{centr} = \frac{1}{4}(\mathbf{X}_i + \mathbf{X}_j + \mathbf{X}_k + \mathbf{X}_l) \quad \text{for atoms } i, j, k, \text{ and } l \quad (30)$$

of both tetrahedra were taken as different initial estimates for the penetrant position at a three-dimensional transition state.

The transition state was refined for each initial guess position by introducing a methane penetrant and performing a three-dimensional transition state search, using the Cerjan-Miller[62] type algorithm described by Baker.[63] This search yielded a three-dimensional transition state, $(x^{\ddagger}_{pen}, y^{\ddagger}_{pen}, z^{\ddagger}_{pen})$, in the space of penetrant positions, the polymer matrix being maintained fixed at its penetrant-free configuration; this process is sketched in Figure 2. Typically this search required ca. 30 s of CPU time on a workstation. Next, the polymer atoms nearest to the penetrant were screened, creating a list of the closest polymer segments (i.e., CH_2 or CH-(CH_3) groups), ordered by increasing distance. The degrees of freedom on the five closest polymer segments were then considered local and flexible. For a segment i neighboring the penetrant, the three bond angles, six torsion angles, and two pendant group bond angles (for a chiral segment) that are on the same chain and surround the segment were chosen to be local and flexible. (See also Figure 1.) Bond angles were included in the list, since molecular dynamics calculations[93] have revealed that excluding them has significant effects on

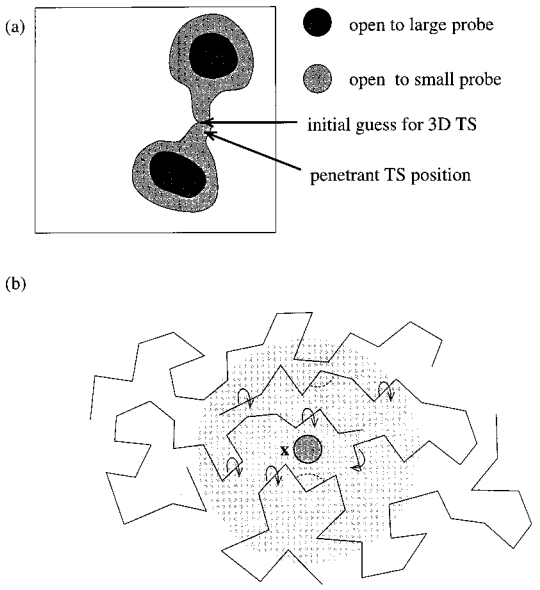

Figure 2. Finding three- and many-dimensional transition states. (a) The space accessible to the small and large probes. The intersections of the holes open to small probes are taken as initial guess sites for a three-dimensional transition state search. (b) The sphere encompassing the flexible generalized coordinates. The diameter of the sphere is increased progressively until the multidimensional saddle point calculation yields asymptotic results. Only some of the flexible degrees of freedom are indicated with arrows and dashed lines.

chain dynamics. A transition state search in this higher-dimensional space (x_{pen}, y_{pen}, z_{pen}, θ_i, ϕ_i, etc.) was then conducted, leading to a revised estimate of the transition state ($x^{\ddagger}_{pen}$, $y^{\ddagger}_{pen}$, $z^{\ddagger}_{pen}$, $\theta^{\ddagger}_i$, $\phi^{\ddagger}_i$, etc.). The polymer atoms nearest to the penetrant atoms were screened again, the degrees of freedom on the 15 nearest polymer segments were added to the list of local, flexible ones, and the transition state in this yet-higher dimensional space was found using Baker's algorithm. This process was continued until (1) all generalized coordinates defined by the segments of atoms i within the cutoff distance of the penetrant−polymer nonbonded potential, $2.45\sigma_{ip}$, from the penetrant were released and (2) release of all generalized coordinates associated with such segments *after* the previous transition state search did not yield any coordinates that were not already local and flexible.[94] At that point, the penetrant position and all polymer degrees of freedom defined by atoms in a spherical region around the penetrant were local and flexible, and the potential energy gradient with respect to all these coordinates equaled zero. Releasing degrees of freedom in this incremental manner was faster computationally than releasing all neighboring degrees of freedom at once. The two methods led to similar transition states that differed in energy by order $O(k_BT)$ or less.

The final result of this procedure was a transition state in penetrant and polymer degrees of freedom for the diffusive jump of a penetrant between two local minima. The resulting multidimensional transition state was a true first-order saddle point: the gradient equaled zero (with respect to all ca. 350 flexible degrees of freedom), and the Hessian matrix had exactly one negative eigenvalue.

The entire transition state search process was repeated for all initial estimates of the penetrant location determined through geometric analysis of each local-

minimum pure polymer configuration. To prevent duplicating previous calculations, a table containing the final penetrant position and the penetrant−polymer interaction energy was recorded for each search in f flexible degrees of freedom, from each initial guess location. This table was scanned after each successful search to see if the new penetrant position and penetrant−polymer energy matched a transition state found previously. If so, the process of increasing the number of flexible degrees of freedom was halted. Such duplicates were found often for three-dimensional transition states, especially for searches starting from both tetrahedra in an intersecting pair. Significant duplicates were found as well for transition states in over 100 degrees of freedom. Duplication of multidimensional transition states at such a high dimensionality suggests that, given a particular region in which the penetrant is located, few chain configurations correspond to transition states, and existence of multiple minimum-energy pathways leading to the same net penetrant displacement is unlikely.

Choice of Flexible Coordinates along the IRC. Having located multidimensional saddle points of the potential energy in the configuration space of the polymer + penetrant system, we proceeded to construct the full reaction path passing through each saddle point. The IRC approach described above was used to track the reaction path in flexible generalized coordinates. On either side, each reaction path terminated at local minima of the potential energy function, which will be termed "states". The local minima were expected to reside somewhere in the geometrically determined sorption states whose intersection point yielded the initial guess position for the penetrant. However, our method of finding a saddle point does not guarantee such a condition.

The penetrant was displaced by O(5 Å) during each diffusive jump; this was a significant fraction of the radius of the sphere that encompassed the flexible segments. Consequently, it was appropriate to rechoose the flexible degrees of freedom along the reaction path. During the calculations following the IRC, the list of flexible degrees of freedom was rechosen each time the penetrant neighbor list was updated, and the number of flexible segments was taken to its asymptotic limit immediately (without iteration). Previously flexible degrees of freedom that were not rechosen were then phased out (i.e., considered bound with infinite stiffness to their new values). Newly chosen flexible degrees of freedom were phased in (i.e., released). The final local minima (the reactant and product states) had a number of common degrees of freedom. The motivation for continuously updating the set of flexible coordinates was to keep the motions local, to keep the problem dimensionality as small as possible (while still realistic), and to prevent long-range conformational relaxation of entire chains.

Implementation of the Harmonic Rate Constant. The rate constant was evaluated for each jump through direct application of eqs 28 and 29 for the classical and quantum-mechanical cases. First, a list was created of the generalized coordinates (degrees of freedom) that were local and flexible anywhere along the entire reaction path. Typically, this list numbered over 500 generalized coordinates. The Hessian was calculated at the local minima and the transition state with respect to these 500 coordinates, and the flexible eigenvalues (and associated frequencies) were calculated with eq 23. For the classical rate, the determinants of the covariant metric tensor in all coordinates, det **a**, and in the flexible coordinates, det $\mathbf{a}^0$, were calculated; det $\mathbf{a}^{-1''}$ was then found through the Fixman relation (eq 62 in Appendix B). The explicit evaluation was performed with matrix routines from the LINPACK library.[95] Care had to be used in evaluating both determinants, since their absolute magnitudes often exceeded 10^{100}. Such a size may seem physically unreasonable but is understandable mathematically: a quantity $l^2 \sin\theta$ (i.e., greater than unity) is being raised to the "number of bonds" power. Only the ratio of these determinants at different locations carries physical significance. Typically, the value of det $\mathbf{a}^{-1''}$ varied by no more than 1% among different conformations.

Macrostate Hypothesis. We undertook the geometric analysis of ref 51 on the assumption that void regions in the polymer matrix that are accessible to a hard sphere probe are more likely to be visited by a soft-sphere penetrant than are regions inaccessible to the probe. However, the shape of each accessible volume cluster (or void) fluctuates with polymer conformation fluctuations, and for each conformation sampled, numerous local minima on the total potential energy hypersurface probably exist for the penetrant within each accessible volume cluster. Each of these local minima may be called a "state", and an accessible volume cluster could be partitioned into a number of individual states. A fluctuating penetrant−polymer system, such as one observed in a molecular dynamics simulation, would visit these different states according to their Boltzmann-weighted probability. The first aspect of the macrostate hypothesis is that these states are separated by energy barriers that are small relative to the thermal energy k_BT, and therefore the time required to move from any one state to another would be small in relation to the time elapsing between passages from one accessible volume cluster to another. Such a collection of penetrant sorption states is termed a macrostate, since the closely residing local minima correspond to different positions for the sorbed penetrant within fairly similar polymer configurations.

The second aspect of the macrostate hypothesis is that distinct macrostates are separated by energy barriers much larger than k_BT. Passage between the macrostates is then an infrequent event, and studying such transitions with transition state theory is appropriate. In principle, the net rate to jump from a macrostate A to a macrostate B equals the sum of all jump rates from individual states in A to individual states in B:

$$p_A k_{A\to B} = \sum_i \sum_j p_A \left(\frac{p_{A_i}}{p_A}\right) k_{A_i\to B_j} \tag{31}$$

where p_A and p_{A_i} denote the equilibrium probabilities of occupying macrostate A and state i within macrostate A, respectively. In most cases, we observed only single jumps between different macrostates, implying that $k_{A_i\to B_j}$ was nonzero for only a single $\{ij\}$ pair, though a few macrostate pairs were connected by multiple paths involving significantly different transition states. All quantitative results in this paper are based on the rate constants $k_{A_i\to B_j}$ between individual states. We distinguish between jumps between macrostates and jumps within a macrostate. Both jump types arose with the initial-estimate strategy used to find penetrant jump

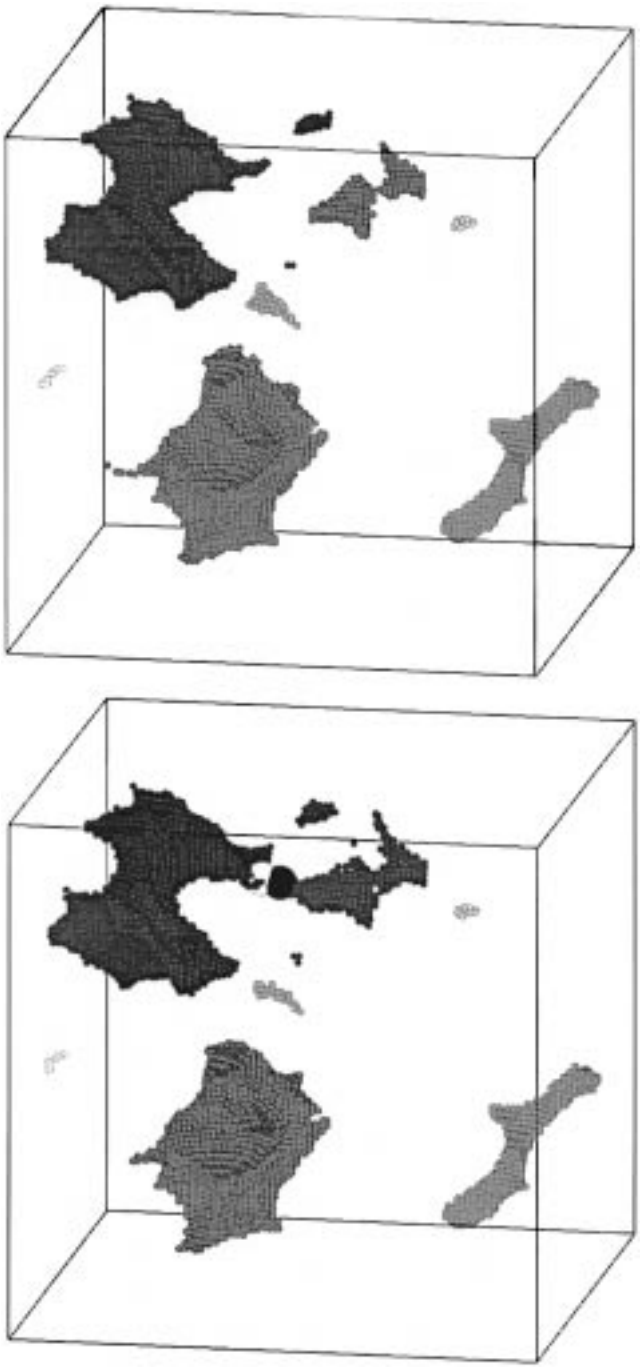

Figure 3. (Top) The volume accessible to a helium probe in an initial (penetrant-free) pure polymer configuration. (Bottom) Same quantity in a configuration rearranged to the transition state for a jump between two voids. The light and dark spheres indicate the initial guess and final value for the penetrant location at the transition state. Different shadings indicate distinct holes, as in ref 51. See text for details.

transition states. Though it is not valid to apply TST to jumps within a single macrostate, those results are included to support the macrostate hypothesis and to provide a basis against which the intermacrostate jump results may be compared.

Results and Discussion

Comparison of the Transition State and the Initial Estimate. The quality of the initial estimate from geometric analysis (for the penetrant position) can be seen for a particular jump in Figure 3. The top

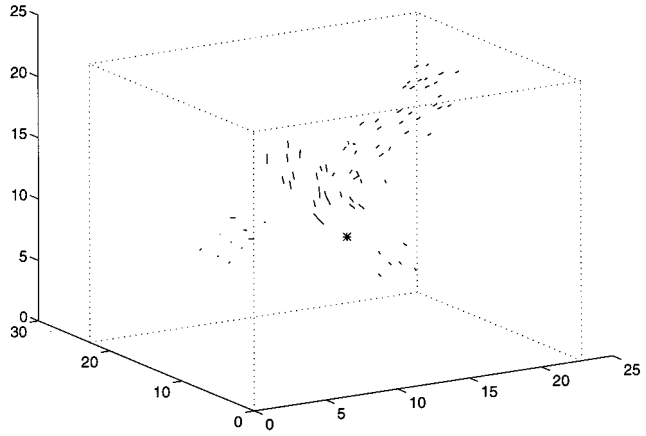

Figure 4. Displacement of heavy atoms between an initial (pure polymer) and a transition state configuration for one particular jump. Only displacements of C atoms and R groups greater than 0.2 Å are shown. The asterisk symbol (*) indicates the penetrant location at the transition state.

picture illustrates the volume accessible to a helium-sized hard sphere probe, using the methods described in ref 51, in one penetrant-free atactic polypropylene microstructure. Different shadings indicate different sorption macrostates; volume excluded by the penetrant is not shown in this figure. The bottom picture depicts the same information, but with the polymer configuration rearranged to the multidimensional transition state found for a penetrant jump between two accessible regions. The three-dimensional initial guess and final multidimensional transition state positions of the methane are indicated by light and dark spheres. The macrostates between which the transition occurs are now labeled with the same shading: the channel between them has widened, and a helium probe could pass between them. The initial guess is very close to the actual transition state position, confirming the utility of the geometric analysis. In this case, the saddle point search located a single transition state between the pair of sorption macrostates. Polymer chain rearrangements to attain the transition state conformation effected an increase in the space available to the penetrant between adjoining voids, and the conformational changes opened a channel through which the penetrant could pass. Similar channel openings were observed in molecular dynamics simulations by Takeuchi,[19] Sok et al.,[36] and Müller-Plathe et al.[50] at temperatures near the glass transition. Such an opening would not be possible in a static matrix, and it is unlikely that concerted opening of such a large hole could be explained solely by independent vibrations of polymer atoms.

Differences between the initial and transition state polymer configurations, depicted in Figure 3 as differences in accessible volume, can also be seen by following how atoms of the polymer displace in order to accommodate the penetrant. Shown in Figure 4 for a different jump are the displacements of carbon atoms and methyl groups whose local minimum and transition state positions differed by more than 0.2 Å. Though changing a single generalized coordinate (such as a bond or torsion angle) would have flailed its entire chain, collective changes among flexible generalized coordinates instead caused local displacements of polymer atoms away from the penetrant. Changes occurred only on atoms in the neighborhood of the penetrant, and local conformational changes were sufficient to accommodate it. In this

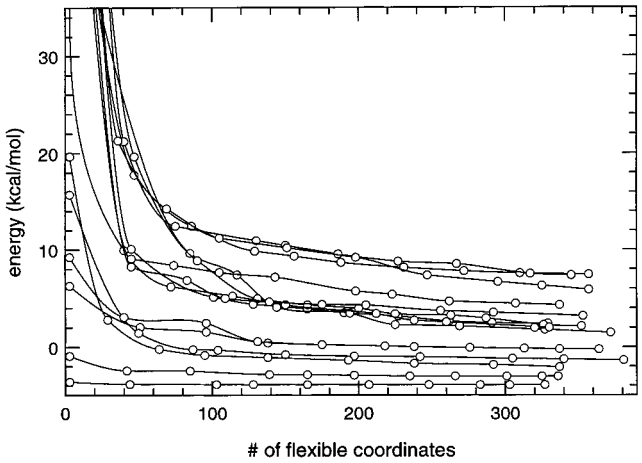

Figure 5. Decrease in transition state energy with increasing number of flexible generalized coordinates for one initial polymer configuration.

particular case, one chain moved out of the way to create space for the penetrant, while two other passing chains moved slightly.

Change in Transition State Energy with Dimensionality. The transition state search procedure involves refinement of the transition state in a progressively increasing number of flexible degrees of freedom. As the dimensionality of the transition state increases, its potential energy decreases. Figure 5 displays the total potential energy of a number of different transition states as a function of increasing number of flexible generalized coordinates. The different curves correspond to a number of different transition state searches within one initial polymer configuration. The potential energy is initially high for methane in this static configuration of polypropylene; however, slight chain rearrangements reduce the energy of the transition state significantly. The penetrant is repositioned during these stages; the gradient equals zero with respect to penetrant position and with respect to all local, flexible polymer degrees of freedom at each point in Figure 5. For diffusion in a crystal, one curve would exist for each type of jump pathway. Many curves are obtained for jumps in a glassy polymer since each channel exhibits slightly different energetics. Each curve terminates at a slightly different number of flexible generalized coordinates due to slight differences in the number of polymer segments that interact with the penetrant (differences in local density). The asymptotic region, in which increasing the number of flexible degrees of freedom no longer affects the transition state energy, is reached before the number defined by all interacting segments. The latter criterion for terminating the transition state search was retained so as to provide an unambiguous selection technique free of "user intervention".

Jump Path Results. The saddle point search process resulted in numerous penetrant jump transition states for each of the six minimum energy polymer structures analyzed. The intrinsic reaction coordinate (IRC) passing through each of the transition states was followed. The resulting path traces approximately how the penetrant position and polymer conformation evolve as the total system passes from the reactant to the product state.

The potential energy along the reaction coordinate for the jumps in Figures 3 and 4 are shown in Figure 6.

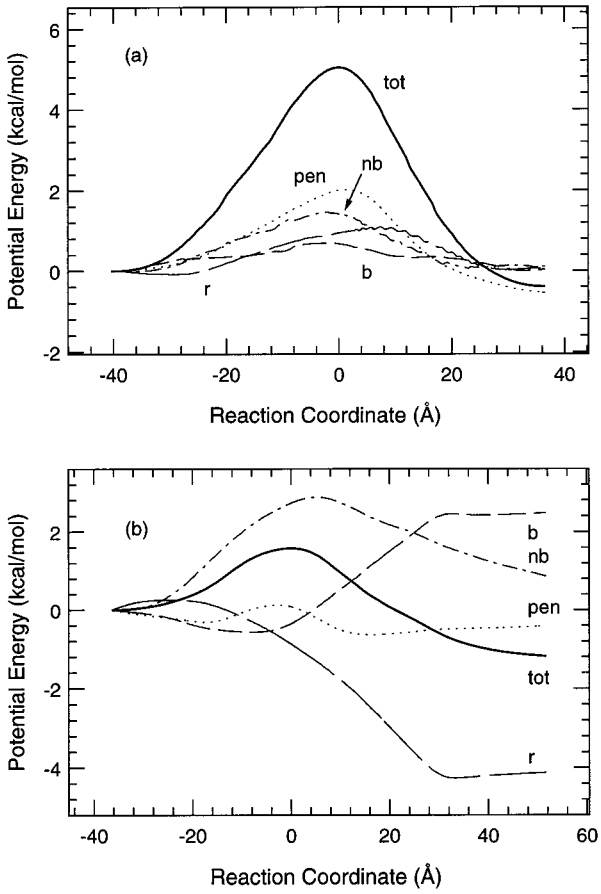

Figure 6. Change in energy along the IRC for the jumps visualized in Figures 3 and 4. The reaction coordinate (abscissa) includes contributions from both penetrant and polymer chain motions.

The reaction coordinate equals the arc length of the curve followed in multidimensional space by the penetrant−polymer system along the IRC (see eq 43), and the zero is defined by the location of the transition state; the reaction coordinate does not equal the net displacement of the penetrant. Different lines indicate contributions from the different terms (eqs 1, 2, and 4) to the potential energy barrier: bond angle bending (b), torsion angle rotation (r), polymer−polymer nonbonded, and penetrant−polymer nonbonded interactions. The roles of different contributions are discussed in ref 17. Energy and position changes along the IRC were smooth, and no discontinuities in the diffusion path were observed when a sufficient number of generalized coordinates were considered local and flexible. The potential energy barriers for these jump events, in the range of several kcal/mol, are significantly larger than the thermal energy k_BT, equal to 0.46 kcal/mol at 233 K, and thus validate one of the underlying assumptions of TST. Though these energy profiles (and associated jump rates and jump lengths) are typical, not all jumps have exactly those energy profiles, jump rates, etc. The distributions observed in a series of simulations are presented and discussed in the next sections. Other jump profiles are shown in ref 17.

Asymptotic Nature of the IRC. So far, the use of a flexible subset of generalized coordinates has only been justified on physical grounds. The goals of this section are to demonstrate that the IRC reaches a steady shape as the number of flexible generalized coordinates increases. Elsewhere[84] we have shown that

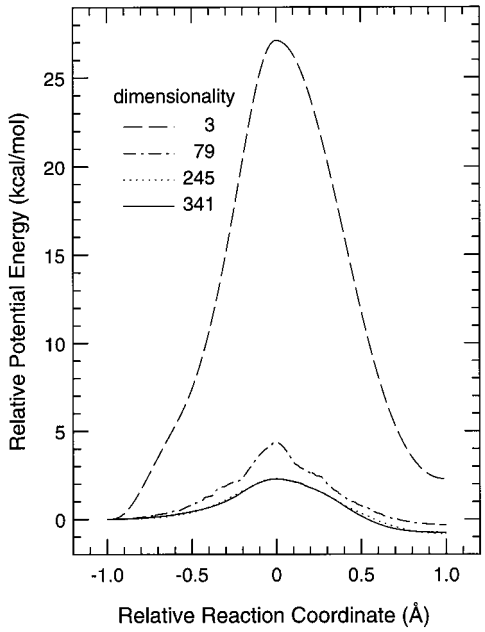

Figure 7. Change in the IRC energy profile with an increasing number of flexible coordinates for the same penetrant jump. From top to bottom, the curves correspond to transition states and diffusion paths in 3, 79, 245, and 341 degrees of freedom. Energies are measured relative to the origin state. The reaction path coordinate on each side of the transition state has been normalized by the arc length from state to transition state in the multidimensional space of generalized coordinates in which each calculation is conducted. Zero corresponds to the transition state, while −1 and +1 to the origin and destination states, respectively.

the calculated jump rate constant is not significantly affected by the method of rechoosing flexible coordinates along the IRC.

Figure 7 displays the energy profile along the IRC as calculated in four different ways for a single jump. The top curve corresponds to the three-dimensional diffusion path through a rigid polymer, such as used in the study by Gusev et al.[58] Subsequent curves correspond to two intermediate numbers of flexible coordinates (79 and 245) and to the ultimate number of flexible coordinates (341) defined by the selection method outlined above. In the intermediate cases, the flexible generalized coordinates were defined by the 15 and 55 segments nearest to the penetrant. The transition state dimensionality equaled the IRC dimensionality for all four cases, and the observed decrease in the transition state energy is in agreement with Figure 5. The energy barrier for the three-dimensional case is 1 order of magnitude larger than for the other cases, leading to a rate 6 orders of magnitude smaller than those of the highly multidimensional cases. This result explains the estimated diffusivity $D \ll 10^{-12}$ cm^2 s^{-1} in a rigid polymer matrix reported in ref 58; there the penetrant was trapped within a state by extremely high energy barriers and could only escape rarely. In the highly multidimensional cases, both the IRC and the rate constant approach an asymptotic limit as the dimensionality increases. This confirms that the method used here for selecting flexible degrees of freedom captures the essential physics of a diffusive jump. A similar dependence was observed by Sonnenburg et al.[27] in their MD study of penetrant diffusion in a rubbery polymer network. There, the diffusivity decreased by 2 orders of magnitude when atoms of the polymer were considered frozen, instead of flexible.

Table 1. Average Properties of Penetrant Jumps[a]

	intermacrostate average		
property	arithmetic	geometric	harmonic
jump rate (μs^{-1})	26 600	0.947	2.96×10^{-11}
jump length (Å)	5.53	5.31	5.08
entropy barrier (k_B)	−4.08		−1.74
potential energy barrier (kcal/mol)	5.73	4.36	1.91
macrostate-to-macrostate jump length	10.31	7.40	0.158

	intramacrostate average		
property	arithmetic	geometric	harmonic
jump rate (μs^{-1})	295 000	16 400	6.60×10^{-3}
jump length (Å)	2.60	1.70	0.526
entropy barrier (k_B)	−2.70		−2.41
potential energy barrier (kcal/mol)	1.85	0.900	0.207

[a] Both inter- and intramacrostate averages are listed for each property; 163 and 45 jumps were used for inter- and intramacrostate averages. The arithmetic mean places more weight on the largest values observed, the geometric mean (implemented as the arithmetic mean of the logarithm) places equal weight on large and small values, and the harmonic mean (the arithmetic mean of the multiplicative inverse) places more weight on the smallest values observed. An arithmetic mean suggests that resistances to transport along single jumps are aligned in parallel, while a geometric mean suggests they are aligned in series. Three significant digits are reported.

Averages and distributions of jump rate constants, jump lengths, energy barriers, and entropy barriers are described in the following sections. A complete set of average results is listed in Table 1. Three types of averages are reported in that table: arithmetic, geometric, and harmonic means. The three are similar in value for narrow distributions and widely disparate for broad distributions.

Rate Constant Distribution. The forward and backward jump rates along each pathway were calculated with a harmonic approximation of the total potential energy hypersurface at the local minima and transition state, using the expressions developed in Appendix B. All degrees of freedom that were considered flexible at any point along the IRC were incorporated in the harmonic approximation; typically, 450−550 generalized coordinates were involved.

The many simulated jumps fall in two sets: intermacrostate and intramacrostate jumps. The first set are those desired for simulating penetrant diffusion, while the second provide support for the macrostate hypothesis. Individual jumps were assigned as inter- or intramacrostate on the basis of whether the penetrant positions at their associated local minima lay in different or in the same accessible volume clusters, using the cluster boundaries found in the initial (energy-minimized) pure polymer structure.

The distribution of inter- and intramacrostate jump rates observed in these simulations is shown in Figure 8. The abscissa contains the jump rate constant on a logarithmic scale, and the ordinate shows the fraction of jumps falling in each bin. The jump rates were calculated by eq 29. Averages are listed in Table 1. Most TST rate constants for the intermacrostate jumps are of order 10^{-3}−10^{3} μs^{-1}, implying very long times on the molecular level. These rates are much slower than those accessible in typical molecular dynamics simulations; a rate of 100 μs^{-1} implies an average waiting time of 10 ns before an event occurs. Presumably, the MD

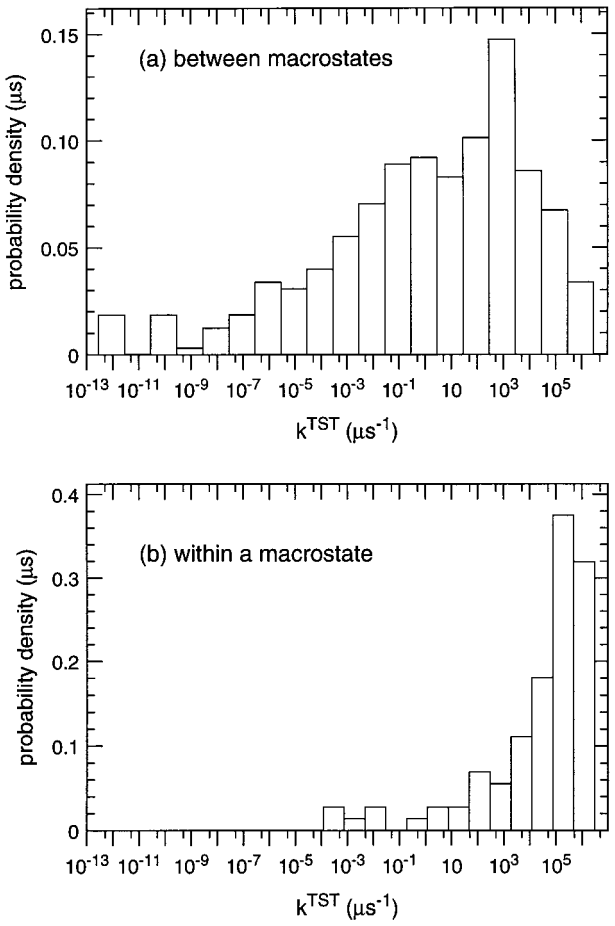

Figure 8. Jump rate constant distributions for (a) inter- and (b) intramacrostate jumps. The distribution is normalized such that $\int p(k^{TST})\, d \log_{10} k^{TST} = 1$.

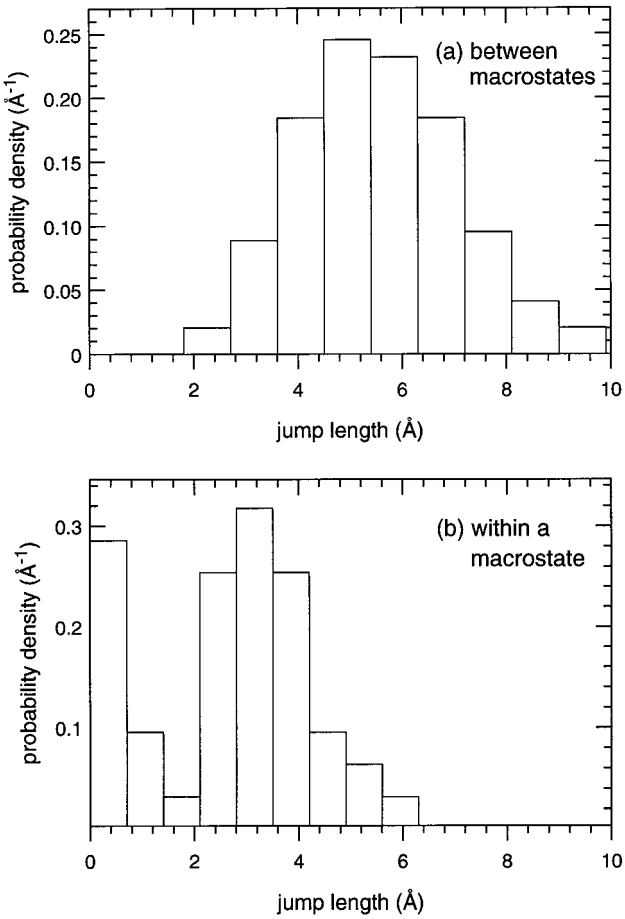

Figure 9. Jump length distributions for (a) inter- and (b) intramacrostate jumps. This jump length equals the penetrant displacement.

simulations described in the Introduction have sampled the faster side of this distribution for their respective penetrant−polymer systems. The advantage of using a stochastic method, such as transition state theory, is that it is not necessary to track the detailed motions between events; only the events themselves are analyzed. Certain intermacrostate jumps have very large rate constants; these jumps have small energy barriers and correspond to escapes from high-energy sorption states.

As proposed by the macrostate hypothesis, jumps within a macrostate occur very quickly. They do not contribute to diffusion, though they do convey some idea of the rate of penetrant motions within a sorption state. Most intramacrostate TST rate constants are between 10^3 and 10^6 μs^{-1} (or 1−1000 jumps per nanosecond), and would be sampled over molecular dynamics time scales. On average, many intramacrostate transitions would have time to occur before an intermacrostate jump occurred.

The distribution of intermacrostate rate constants spans a much larger range than that calculated by Gusev et al.[39,58,59] For example, the residence times (comparable to the inverse of a jump rate constant) that they calculated at 300 K in polyisobutylene were smaller than nanoseconds. Their escape-time distribution was assumed to be independent of temperature[39] and is relatively independent of the smearing factor.[59] However, Gusev et al. do not distinguish between inter- and intramacrostate jumps, despite recognizing such a pattern in their jump rates.[58] This suggests that the majority of jumps that contributed to their plotted distributions were of the intramacrostate variety. The intermacrostate jumps, though few in number, would have contributed the main resistances to penetrant diffusion over long time scales. One explanation for the slower jump rates found here could be that nonelastic mechanisms contribute to penetrant diffusion over time scales longer than those affected by elastic motions; such a question could be investigated theoretically by applying the Gusev−Suter methodology to the slower of the jumps simulated here.

Jump Length Distribution. The jump length equals the penetrant displacement between the reactant and product states. This length corresponds to the net distance traveled by the penetrant in three-dimensional space, rather than to the length of the curvilinear path traversed by the penetrant between the reactant and product states. This length also differs from the total distance in multidimensional space traveled along the reaction coordinate; motions of both penetrant and polymer atoms contribute to the distance along the IRC, as described in eq 43. For example, if a methyl group moved sideways to create a larger opening for the penetrant, that displacement would add to the reaction coordinate.

Average jump lengths are listed in Table 1, and the distributions of jump lengths observed are shown in Figure 9. The abscissa contains the jump lengths on a linear scale. In contrast to the distribution of jump rates, the jump length distribution is fairly narrow, with most jumps displacing the penetrant by 4−8 Å. Jumps

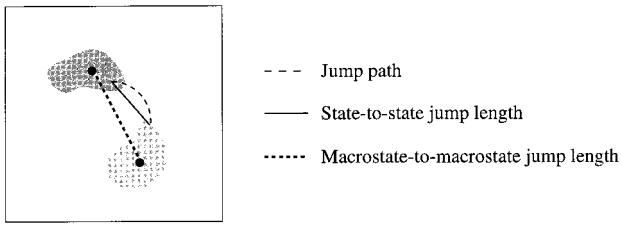

Figure 10. Pictorial definition of the macrostate-to-macrostate jump length. Though the cartoon is drawn in only two dimensions, the quantities depicted are actually three-dimensional. The macrostate-to-macrostate jump length connects the centers of two adjoining sorption macrostates.

within a macrostate are only slightly smaller (2−4 Å), suggesting that distances between macrostates are comparable to the sizes of macrostates themselves. True dynamical trajectories across the low energy barriers of intramacrostate transitions would also explore distances comparable to the length of intermacrostate jumps.

Macrostate-to-Macrostate Jump Lengths. The jump lengths discussed above refer to jumps between individual states, and not entire macrostates—the end points of the different jumps out of a single sorption macrostate do not coincide. Individual jumps do not connect to one another to form a network and consequently do not form connected paths across the polymer structure. If the jump lengths were significantly larger than the sizes of sorption macrostates, the small distances between end points could be ignored. However, as suggested by Figures 3 and 9, the jump lengths between macrostates are comparable in size to the macrostates themselves.

Since motions within a sorption macrostate are fast, a more relevant jump length is what we term the macrostate-to-macrostate jump length, equal to the three-dimensional distance between the centers of the two macrostates connected by a penetrant jump. The network of three-dimensional macrostate-to-macrostate jumps percolates space. The center of each macrostate is best defined by the Boltzmann-weighted average residence point for a penetrant inside it; this could be calculated as the average penetrant position in the course of a MD simulation, during which the penetrant originates in the sorption macrostate of interest. If the penetrant escaped to another sorption macrostate during a short simulation, an infrequent event hypothesis would be invalid for the pair. The centroid of the sorption macrostate, calculated as a volume-weighted average over the centroids of the tetrahedra that comprised the accessible cluster (as in ref 51), serves as an approximate center and was used in the calculations below. Pictorial definitions of the individual and macrostate-to-macrostate jump lengths are shown in Figure 10.

The distribution of macrostate-to-macrostate jump lengths is shown in Figure 11. No plot is shown for jumps that remain within a macrostate; by definition their macrostate-to-macrostate jump length equals zero. Dotted lines indicate different distributions obtained by changing the bin size used when combining the raw data. The thick solid line indicates the distribution chosen for use in subsequent studies.[84] The average macrostate-to-macrostate jump is significantly larger than the average jump length; this is because the former includes distances that would be traveled within the sorption macrostate. The distribution of macrostate-to-macrostate jump lengths is significantly broader as well; the variation in the distance between the jump end point and the macrostate centroid is responsible for the change.

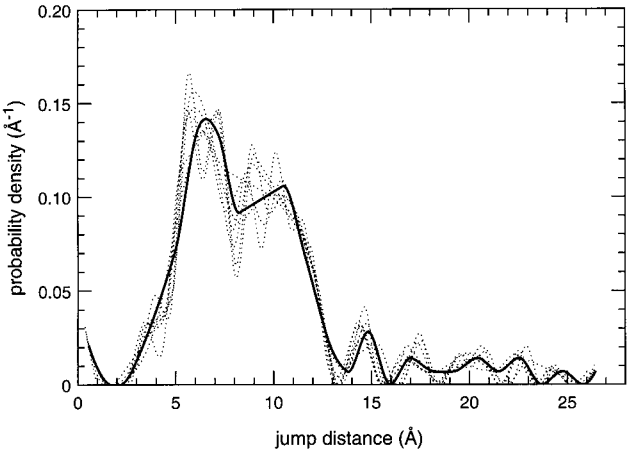

Figure 11. Distribution of macrostate-to-macrostate jump lengths for penetrant jumps between different sorption macrostates. A set of macrostate-to-macrostate jumps connect to one another in a way such that they completely percolate three-dimensional space. Dotted lines indicate the range of distributions consistent with the raw simulation data.

Potential Energy Barrier Distribution. The potential energy barrier to escape from a state over a transition state equals the difference in potential energy between the transition state and the local minimum of origin. This barrier must be significantly larger than the thermal energy k_BT for a TST methodology to be appropriate.

The distributions of potential energy barriers for jumps between and within sorption macrostates are plotted in Figure 12. The energy barriers for jumps within a macrostate are fairly small. The energy barriers for jumps between macrostates are distributed over a very wide range. Jumps with the largest energy barriers have exceedingly small rate constants of order ms^{-1} or s^{-1}. Such jumps would not contribute significantly to penetrant diffusion; if the connectivity of macrostates is high enough, they would be circumvented by successions of faster jumps.

Similar distributions of energy barriers have been observed in other systems. Applying instantaneous normal-mode analysis[96] to a monatomic supercooled liquid, Keyes[97] found that self-diffusivity was governed by a distribution of energy barriers, and he calculated the contribution of each barrier type with transition state theory. The energy barrier distribution, Figure 13 in ref 97, resembles to some extent the one found here for methane in atactic polypropylene. Straub and Thirumalai observed similar results in their molecular simulation of protein dynamics.[98] In those cases, the energy barriers were fit by expressions resembling

$$p(\Delta V) = c_1^2 \Delta V \exp(-c_1 \Delta V) + c_2 \exp(-c_2 \Delta V) \quad (32)$$

with each term used as a basis function for an inverse Laplace transform procedure. Such fits to our results (using the first term for intermacrostate jumps and the second term for intramacrostate jumps) are indicated by dashed lines. The general shapes are somewhat appropriate, but uncertainties in the distributions overwhelm subtle shape aspects.

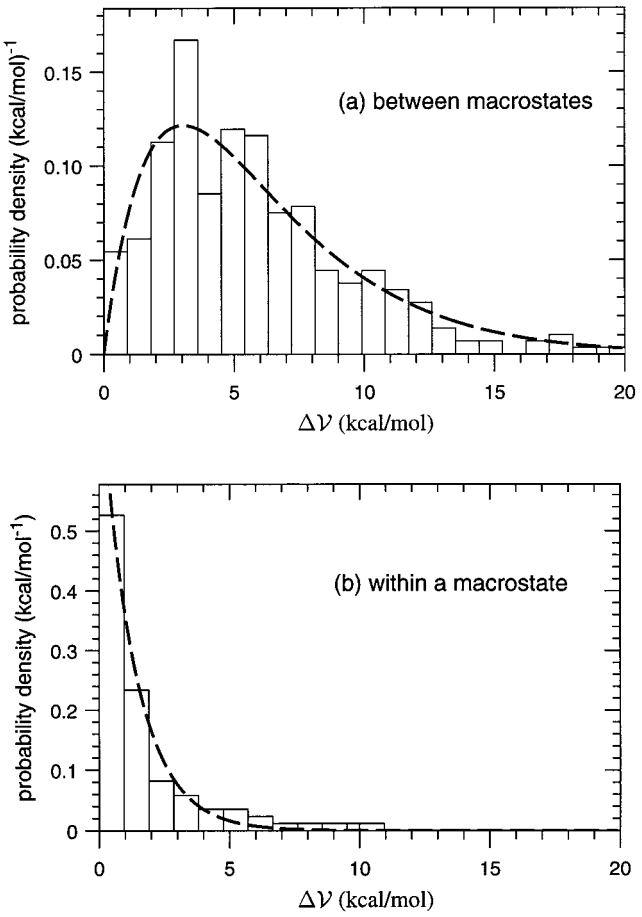

Figure 12. Distribution of potential energy barriers for jumps (a) between and (b) within sorption macrostates. The dashed lines indicate the functions (a) $c_1^2 x \exp(-c_1 x)$, with $c_1 = 0.33$, and (b) $c_2 \exp(-c_2 x)$, with $c_2 = 0.78$; see text for details.

Keyes[97] found that the energy barrier distribution strongly influenced the magnitude and temperature dependence of the supercooled liquid self-diffusivity: D depended much more weakly on T than exponentially with $1/T$ (an Arrhenius dependence). Introducing a low-energy cutoff to the energy barrier (in his theory) modified the temperature dependence again such that it matched those proposed for diffusion and flow among a distribution of energy barriers (a "rough" potential).[99,100] Though different temperatures were not investigated here, the similarities in the energy barrier distributions suggest that anomalies may exist in the extremely low-temperature diffusive behavior of small molecule penetrants in glassy polymers. However, the common description of experimental diffusivities using an Arrhenius form would mean that jumps with high energy barriers do not occur in sufficient numbers at temperatures below the glass transition to impact the diffusivity. This suggests that the shape of Figure 12 ceases to matter above some certain barrier energy.

Entropy Barrier Distribution. The entropy difference between the reactant and transition states represents a difference in the number of probable configurations near each point. In the harmonic approximation, the number of configurations is related to the local curvature of the potential energy hypersurface. In a region with large curvature along directions orthogonal to the IRC, small changes in position and configuration would lead to large increases in potential energy and concomitant decreases in probability, resulting in a small number of probable configurations. In a region with small curvature, there would be little energetic cost to explore regions away from the IRC. The probability of doing so would be higher, as would the number of probable configurations and hence the entropy.

Following ideas of Starkweather,[101] an expression for the entropy barrier may be derived by comparing two forms for the rate constant. The initial form, eq 26, involved the free energy barrier; the final forms, eqs 28 and 29, involved an energy barrier and harmonic frequencies at the initial and the transition states. Representing the frequency-containing prefactor as k_0 and equating the two expressions,

$$k^{\mathrm{TST}} = k_0 \exp\left(-\frac{\Delta V}{k_B T}\right) = \frac{k_B T}{h} \exp(-\Delta A/k_B T) = \frac{k_B T}{h} \exp(\Delta S_a/k_B) \exp(-\Delta E_a/k_B T) \quad (33)$$

where the free energy barrier has been replaced by entropy and internal energy barriers. The barriers in potential energy ΔV and internal energy ΔE_a are related through the temperature dependence of the rate (neglecting the temperature dependence of k_0):

$$\Delta V = -k_B \frac{\partial \ln k^{\mathrm{TST}}}{\partial(1/T)} \quad (34)$$

$$\Delta E_a = \frac{\partial(\Delta A/T)}{\partial(1/T)} = -k_B \frac{\partial \ln(k^{\mathrm{TST}}/T)}{\partial(1/T)} = -k_B\left[\frac{\partial \ln k^{\mathrm{TST}}}{\partial(1/T)} + \frac{\partial \ln(1/T)}{\partial(1/T)}\right] = \Delta V - k_B T \quad (35)$$

Next, a relation between the entropy barrier ΔS_a and the prefactor k_0 is found by substituting for the internal energy barrier and the rate constant in eq 33,

$$\Delta S_a/k_B = \Delta E_a/k_B T + \ln(h k^{\mathrm{TST}}/k_B T) \quad (36)$$

$$= \Delta V/k_B T - 1 + \ln[(h/k_B T) k_0 \exp(-\Delta V/k_B T)] \quad (37)$$

$$= \ln\left(\frac{h k_0}{k_B T}\right) - 1 \quad (38)$$

Recalling the form of the prefactor k_0 for the classical and quantum-mechanical Hamiltonians, the final result indicates that changes in entropy are related logarithmically to changes in normal-mode frequencies between the local minimum and the transition state.

The distribution of entropy barriers, calculated using the quantum-mechanical vibrational partition function, is shown in Figure 13 for jumps between and within sorption macrostates. An entropy loss equal to a few k_B accompanied each diffusion jump. The spread in entropy barriers accounts in most cases for a three-order of magnitude variation in the jump rate constant.

Correlations between the energy and entropy activation barriers are shown in Figure 14. High potential energy barriers tended to occur in conjunction with activation entropies of large (negative) magnitude, though the correlation was not perfect. The variety of entropies observed for a particular activation energy

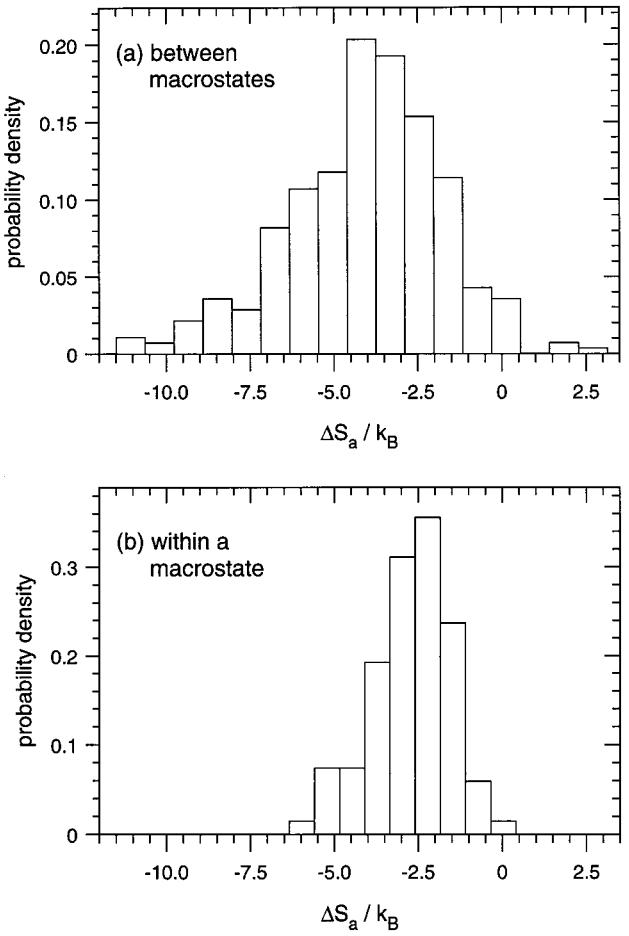

Figure 13. Distribution of entropy barriers for jumps (a) between and (b) within sorption macrostates. The more negative the entropy barrier, the larger the decrease in curvature between the initial and transition states.

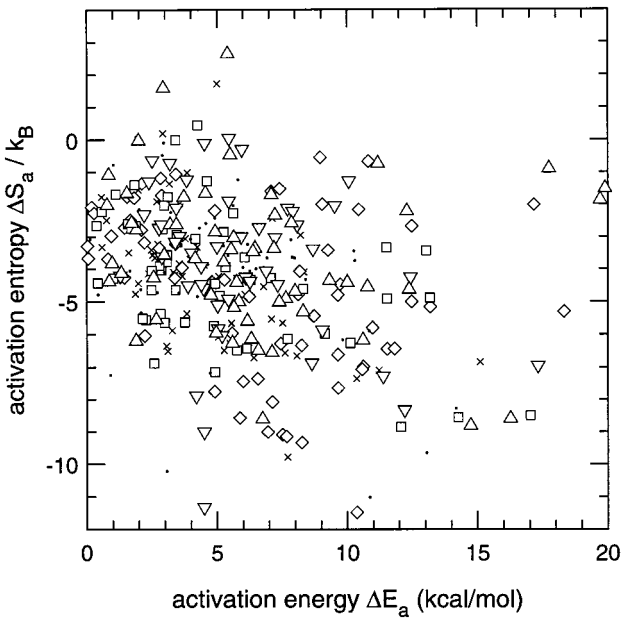

Figure 14. Correlation between activation energy and entropy for intermacrostate jumps. Each point indicates the potential energy barrier (*x*-axis) and activation entropy (*y*-axis) for a single jump. Different symbols indicate jumps based on different initial polymer configurations.

(and vice versa) would lead to jump rate constants spanning a range a few orders of magnitude wide.

Diffusion Coefficient. Although a detailed procedure for calculating the diffusion coefficient for methane in atactic polypropylene will be presented in a later publication, a rough estimate can be made from the averages reported in Table 1. Using the geometric mean of the jump rate (since diffusion occurs via sequences of uncoupled jumps in series) and the arithmetic mean of the macrostate-to-macrostate jump length, in combination with the form of the diffusion coefficient for isotropic jumps on a simple cubic lattice,[102]

$$D = \frac{1}{2d}kl^2 = \frac{1}{2(3)}(0.947\ \mu s^{-1})(10.31\ \text{Å})^2 = 1.7 \times 10^{-9}\ \text{cm}^2\ \text{s}^{-1}$$

which is reasonable for small-molecule diffusivity in a glassy polymer. In a future publication, the entire jump rate constant distribution, the connectivity of the macrostate network, and the spatial and rate correlations between jumps, as obtained from the polymer simulations presented here, will be incorporated into a more elaborate mesoscopic calculation of the diffusivity.

Conclusions

A rigorous formulation has been developed for conducting multidimensional transition state theory calculations in model polymer systems. The basic picture that emerges from the calculations presented here is that a penetrant in a glassy polymer spends most of its time overcoming small energy barriers and rattling within a sorption macrostate. Infrequently, over time scales that range between nanoseconds and milliseconds, polymer conformation fluctuations couple in manners that allow a penetrant to hop between two macrostates. The length scale of this hop, 5−10 Å, is commensurate with the size of the sorption macrostates themselves.

The path in configuration space taken by a diffusing penetrant was described in a flexible subset of the generalized coordinates; the remaining generalized coordinates were governed by harmonic potentials with infinitely stiff force constants. The nonorthogonal generalized coordinates commonly involved in representing polymer chains—bond lengths, bond angles, and torsion angles—necessitated introducing the metric tensor and other concepts of Riemannian geometry. The IRC equation for tracking the reaction coordinate (eqs 17 and 25) was written in a constrained subset of generalized coordinates, as was the initial step away from the transition state. The path followed by the constrained system was independent of the classical statistical mechanical model used to represent the polymer chains.

An equation for the penetrant jump rate constant between sorption states was derived by combining multidimensional transition state theory with a harmonic approximation for the potential energy at the local minima and the transition state. The resulting equation incorporated the flexible model for polymer conformation statistical mechanics in the limit of infinite stiffness for all bond lengths and nonlocal bond and torsion angles. Using a classical form of the Hamiltonian, the rate constant included a contribution from the difference in frequencies of the infinitely stiff modes between transition state and origin state. This contribution became unity when using a quantum-mechanical form of the Hamiltonian.

These methods were applied to methane diffusion in glassy atactic polypropylene at $T = 233$ K. Transition states in penetrant and polymer degrees of freedom were found using the necks of geometrically accessible channels as initial guesses; typically of order 350 degrees of freedom were required to specify the transition state conformation in a manner such that the rest of the polymer configuration remained undisturbed. As the number of included degrees of freedom increased to that point, the transition state energy decreased until an asymptotic limit was reached. Energy profiles along diffusion paths exhibited the same asymptotic behavior.

The rate constant distribution for penetrant jumps between macrostates was very broad, ranging between 10^{-12} and 10^{6} μs^{-1}. The corresponding distribution for jump rates within a macrostate ranged from 10^{-3} to 10^{6} μs^{-1}, showing that a partial, but not complete, separation of time scales exists between inter- and intramacrostate jumps. It was not possible to quantify the inherent systematic errors that were introduced by the harmonic treatment of fluctuations away from the local minimum and transition state.

The jump length distributions for both state-to-state and macrostate-to-macrostate jumps were fairly narrow and were centered about 5 and 7 Å, respectively, for jumps between macrostates. Jump lengths within a macrostate were peaked at about 3 Å. Some overlap occurred between the intramacrostate and intermacrostate distributions of jump lengths.

Distributions of activation energies and entropies for penetrant jumps each spanned about 2 and 1 orders of magnitude in units of $k_B T$ and k_B, respectively. The shape of the energy barrier distribution for intermacrostate jumps resembled an xe^{-cx} distribution peaked at about 5 kcal/mol, with a long tail exceeding 15 kcal/mol. Its width was largely responsible for the breadth of the jump rate distribution. The entropy barrier distribution more closely resembled a symmetric Gaussian peak. A weak negative correlation was found between activation energy and activation entropy for the jumps, large positive activation energies tending to appear together with large negative activation entropies.

On the basis of a separation of time scales, we proposed a macrostate hypothesis: different states within a sorption macrostate would be visited on time scales faster than those of penetrant diffusion, while transitions between macrostates would control the rate of the overall diffusion process. The jump rate constant distributions demonstrated the validity of this hypothesis to a large (but not complete) extent. As mentioned above, the tails of the inter- and intramacrostate distributions overlapped slightly, showing that the time scale separation is diffuse, rather than complete.

The wealth of information calculated here confirmed that an infrequent jump picture remains relevant for describing the moderate time-scale behavior of a small gas (methane) in a glassy amorphous polymer (atactic polypropylene). Polymer chain segments contribute significantly to penetrant dynamics over molecular length scales, and their exclusion would have affected the calculated results by orders of magnitude. The distribution of jump rate constants spans a wide range of time scales. The detailed topological and rate information on intermacrostate jumps, as accumulated by the present study, can be used to construct a coarse-grained model for predicting the long-time diffusive progress of the penetrant as a succession of jumps in a network of macrostates by kinetic Monte Carlo techniques. How this hierarchical modeling is implemented will be discussed in a forthcoming publication.

Acknowledgment. We thank Edie Sevick for many suggestions during the beginning of this work. We also thank Professor Robert Gilbert and Richard Henchman for very stimulating conversations during their visits to Berkeley and Patras in the summer and fall of 1995.

Appendix A. Reduction in Dimensionality of the Transition State and IRC

To remove stiff coordinates from the transition state and IRC expressions, it is necessary to derive forms of the transition state criterion and the IRC equation in which the individual terms span a subset of the full dimensionality of the system. Transforming the vectors $d\mathbf{q}$ and $\nabla_{\mathbf{q}} V$ is straightforward. The total step

$$d\mathbf{q} = \begin{pmatrix} d\mathbf{q}_f \\ d\mathbf{q}_s \end{pmatrix}$$

can be partitioned into flexible ($d\mathbf{q}_f$) and stiff ($d\mathbf{q}_s$) components, since changes made along the flexible coordinates do not affect the stiff coordinates. The gradient vector

$$\nabla_{\mathbf{q}} V = \begin{pmatrix} \nabla_{\mathbf{q}_f} V \\ \nabla_{\mathbf{q}_s} V \end{pmatrix}$$

can be partitioned similarly, since a partial derivative $\partial V/\partial q^i$ is taken with all q^j ($j \neq i$), including the stiff coordinates, held constant.

The Jacobian matrix for transforming from mass-weighted Cartesian to generalized coordinates can be transformed in a manner similar to that used for transforming the potential energy gradient. A derivative $\partial x^k/\partial q^\alpha$ is taken with respect to flexible generalized coordinate q^α while all other generalized coordinates are held constant, so stiff generalized coordinates do not change along the direction $\partial \mathbf{x}/\partial q^\alpha$. Thus the Jacobian matrix J' may be partitioned as

$$J' = \begin{pmatrix} \partial x^1/\partial q^1 & \cdots & \partial x^1/\partial q^f & \partial x^1/\partial q^{f+1} & \cdots & \partial x^1/\partial q^{3N} \\ \vdots & & \vdots & \vdots & & \vdots \\ \partial x^{3N}/\partial q^1 & \cdots & \partial x^{3N}/\partial q^f & \partial x^{3N}/\partial q^{f+1} & \cdots & \partial x^{3N}/\partial q^{3N} \end{pmatrix} = (J'_f\, J'_s) \quad (39)$$

and J'_f and J'_s are rectangular $3N \times f$ and $3N \times (3N - f)$ matrices, respectively; this nomenclature is similar to that of Gō and Scheraga.[90]

Transforming the metric tensor is more difficult. Fukui[64] reduced the dimensionality to $3N - 6$ by removing translation and rotation. However, rotation cannot be removed when using periodic boundary conditions, and neither can be removed in the presence of an external potential, such as interactions with other chains. Furthermore, the resulting system would still contain a large number of degrees of freedom, such as bond lengths, which are infinitely stiff in the polymer system here. Weiner (section 6.31 of ref 85) has outlined how the number of degrees of freedom can be reduced significantly. He addressed a system subject to geometric constraints by choosing a subset q^α, $\alpha = 1, \ldots, f$,

to be flexible; the remaining degrees of freedom q^A, $A = f + 1, ..., 3N$, were constrained to their equilibrium values. Next, he calculated (p 217 of ref 85) the covariant metric tensor for the reduced space by subdividing the covariant metric tensor of the entire space

$$\mathbf{a} = \left(\begin{array}{c|cc} \mathbf{a}^0 & \mathbf{a}' \\ \hline \mathbf{a}'^{\mathrm{T}} & \mathbf{a}'' \end{array}\right) \tag{40}$$

into submatrices $\mathbf{a}^0$, $\mathbf{a}'$, $\mathbf{a}'^{\mathrm{T}}$, and $\mathbf{a}''$; the $f \times f$ element $\mathbf{a}^0$ in the upper left is the covariant metric tensor in the flexible coordinates. Each element

$$\mathbf{a}_{\alpha\beta} = \sum_k \frac{\partial x^k}{\partial q^\alpha}\frac{\partial x^k}{\partial q^\beta}$$

is unaffected when q^α and q^β remain flexible, since constrained generalized coordinates (such as q^A) were already held constant implicitly when taking the partial derivatives. The elements of $\mathbf{a}^0$ are related to the Jacobian matrix in the reduced dimensionality by

$$\mathbf{a}^0 = J'^{\mathrm{T}}_{\mathrm{f}} J'_{\mathrm{f}} \tag{41}$$

using the subsets of the Jacobian introduced above. The contravariant metric tensor of the reduced space is *not* a submatrix of the contravariant metric tensor in the full space, $\mathbf{a}^{-1}$, since the partial derivatives that would define each term are taken with all other mass-weighted Cartesian coordinates held constant, not all other generalized coordinates. Instead, the reduced-space contravariant metric tensor must be found as a matrix inverse in the reduced dimensionality or by eq 10 of ref 90.

Transition State. For nonflexible degrees of freedom $A = f + 1, ..., 3N$, the restoring potential maintaining the constraints is of the form $V^{\mathrm{stiff}} = \sum_A {}^1/_2 k_{\mathrm{stiff}_A}(q^A - q_0^A)^2$, with each k_{stiff_A} conceptually taking on values that approach infinity.[90] The elements of the gradient $\nabla_{\mathbf{q}} V$ corresponding to stiff degrees of freedom contain contributions of the form $\partial V^{\mathrm{stiff}}/\partial q^A = k_{\mathrm{stiff}}(q^A - q_0^A)$. At a stationary point (minimum or saddle point), where $\nabla_{\mathbf{q}} V = 0$, each q^A must necessarily assume its equilibrium value q_0^A. The Hessian submatrix associated with the constrained degrees of freedom takes on a diagonal form, with eigenvalues given by the stiff spring constants, which approach infinity. Since all these eigenvalues are positive, it is meaningful mathematically to discuss the transition state with respect to a flexible subset of generalized coordinates.

A saddle point in this system of reduced dimensionality is thus a point at which each element of the potential energy gradient equals zero for all flexible generalized coordinates q^α (eq 22 above), and each eigenvalue of the Hessian with respect to the subset of flexible generalized coordinates is positive except for the lowest, which must be negative. The exact form of the eigenvalue equation to solve follows shortly.

IRC Steps Not at the Transition State. The prescription for steps along the IRC in a subset of generalized coordinates follows from eq 17 by partitioning $\mathbf{a}$, $\mathrm{d}\mathbf{q}$, and $\nabla_{\mathbf{q}} V$ into flexible and stiff parts. The infinitely stiff springs maintain $\mathrm{d}q^A = 0$ for each stiff coordinate A. The elements of $\mathbf{a}$ that multiply the subvector of flexible $\mathrm{d}q^\alpha$ correspond exactly to the submatrix $\mathbf{a}^0$. Similarly, only the gradients with respect to flexible generalized coordinates are nonzero, since the gradient with respect to stiff degrees of freedom equals zero in either the rigid or the infinitely stiff model. The resulting prescription, eq 25 in the main text, was used for tracking the IRC. At a given point in configuration space, the covariant metric tensor $\mathbf{a}^0$ was calculated in the subset of flexible coordinates. Next, the gradient was calculated with respect to the flexible degrees of freedom, and the step direction $\mathrm{d}\mathbf{q}_{\mathrm{f}}$ was calculated with eq 25. The factor $\mathrm{d}\tau$ was used to increase or decrease the step magnitude. After 15 steps in which the predicted and actual change in energy agreed within $<10^{-3}$ kcal/mol, the step magnitude $|\mathrm{d}\mathbf{q}^{\mathrm{T}}\mathbf{a}^0\mathrm{d}\mathbf{q}|$ was increased by a factor of ${}^5/_4$. If the energy agreement was poorer than 10^{-3} kcal/mol, the step size was decreased immediately by the same factor; if agreement was poorer than 10^{-2} kcal/mol, the step size was decreased by $({}^5/_4)^2$ and the step itself was repeated.

The change in distance s along each step was defined by

$$\mathrm{d}s^2 = \sum_i (\mathrm{d}x^i)^2 \tag{42}$$

Substituting for each $\mathrm{d}x^i$ using eq 11, restricting $\mathrm{d}\mathbf{q}$ to flexible generalized coordinates, and simplifying with the flexible part of the covariant metric tensor lead to

$$\mathrm{d}s^2 = \mathrm{d}\mathbf{q}_{\mathrm{f}}^{\mathrm{T}}\mathbf{a}^0\,\mathrm{d}\mathbf{q}_{\mathrm{f}} \tag{43}$$

where $\mathrm{d}\mathbf{q}_{\mathrm{f}}$ contains only the changes in the local, flexible degrees of freedom. Equation 43 was used to calculate the distance along the IRC as each jump path was followed.

Step from the Transition State. As in the full dimensionality, the first step is directed along the eigenvector corresponding to the negative eigenvalue. After partitioning the contravariant metric tensor $\mathbf{a}^{-1}$ along the same lines as in eq 40, premultiplying eq 21 by $\mathbf{a}^{-1}$ leads to

$$\begin{pmatrix} \mathbf{a}^{-1^0} & \mathbf{a}^{-1'} \\ \mathbf{a}^{-1'^{\mathrm{T}}} & \mathbf{a}^{-1''} \end{pmatrix}\begin{pmatrix} \mathbf{H}^0_{qq} & \mathbf{H}'_{qq} \\ \mathbf{H}'^{\mathrm{T}}_{qq} & \mathbf{H}''_{qq} \end{pmatrix}\begin{pmatrix} \mathbf{q}'_{\mathrm{f}} \\ \mathbf{q}'_{\mathrm{s}} \end{pmatrix} = \lambda \begin{pmatrix} \mathbf{q}'_{\mathrm{f}} \\ \mathbf{q}'_{\mathrm{s}} \end{pmatrix} \tag{44}$$

where $\mathbf{q}'_{\mathrm{f}}$ and $\mathbf{q}'_{\mathrm{s}}$ indicate the flexible and infinitely stiff components of the eigenvector $\mathbf{q}'$. Matrix multiplication leads to two equations,

$$(\mathbf{a}^{-1^0}\mathbf{H}^0_{qq} + \mathbf{a}^{-1'}\mathbf{H}'^{\mathrm{T}}_{qq})\mathbf{q}'_{\mathrm{f}} + (\mathbf{a}^{-1^0}\mathbf{H}'_{qq} + \mathbf{a}^{-1'}\mathbf{H}''_{qq})\mathbf{q}'_{\mathrm{s}} = \lambda\mathbf{q}'_{\mathrm{f}} \tag{45}$$

$$(\mathbf{a}^{-1'^{\mathrm{T}}}\mathbf{H}^0_{qq} + \mathbf{a}^{-1''}\mathbf{H}'^{\mathrm{T}}_{qq})\mathbf{q}'_{\mathrm{f}} + (\mathbf{a}^{-1'^{\mathrm{T}}}\mathbf{H}'_{qq} + \mathbf{a}^{-1''}\mathbf{H}''_{qq})\mathbf{q}'_{\mathrm{s}} = \lambda\mathbf{q}'_{\mathrm{s}} \tag{46}$$

The matrix $\mathbf{H}''_{qq}$ is the sum of the second derivative matrices, with respect to two stiff generalized coordinates, of the nonbonded interactions and the harmonic stiffness interactions. Since the stiffness is harmonic, the diagonal terms of $\mathbf{H}''_{qq}$ equal the force constants, which approach infinity in the limit of infinite stiffness. The nondiagonal terms are small and finite,[76] since they only depend on changes in the nonbonded energy or are governed by force constants that remain finite. In this sense, the system under consideration is "more" block-diagonal than that of Lazaridis et al.,[76] since the force

constants here actually approach infinity, rather than remaining merely large and finite. The elements of $\mathbf{H}^0_{qq}$ and $\mathbf{H}'_{qq}$ remain finite as the force constants associated with $\mathbf{q}_s$ approach infinity, as do the elements of the $\mathbf{a}^{-1}$ submatrices. For eq 45 to hold with finite λ and $\mathbf{q}_f$, we must necessarily have $\mathbf{q}'_s \rightarrow \mathbf{0}$ for all stiff coordinates of an eigenvector with a finite eigenvalue. Even with the force constants approaching infinity, the right-hand side of eq 46 approaches zero, as does the second term on the left-hand side of the same equation. Since the step $\mathbf{q}'_f$ in the flexible coordinates is nonzero, for eq 46 to be satisfied the metric tensor submatrices and the Hessian submatrices must be related such that

$$\mathbf{a}^{-1''}\mathbf{H}'^{\mathrm{T}}_{qq} = -\mathbf{a}^{-1'^{\mathrm{T}}}\mathbf{H}^0_{qq}$$

After solving for $\mathbf{H}^{T}_{qq}$ in this limit and substituting the result into eq 45, rearrangement leads to

$$[\mathbf{a}^{-1^0} - \mathbf{a}^{-1'}\mathbf{a}^{-1''^{-1}}\mathbf{a}^{-1'^{\mathrm{T}}}]\mathbf{H}^0_{qq}\mathbf{q}'_f = \lambda\mathbf{q}'_f \qquad (47)$$

The factor in brackets equals the inverse of $\mathbf{a}^0$ (from ref 90), and premultiplying by $\mathbf{a}^0$ leads to eq 23.

What happens to the eigenvalues corresponding to the infinitely stiff degrees of freedom? The original Hessian has $3N$ eigenvalues, while the Hessian in the restricted (flexible) coordinate system has only f eigenvalues. The "loss" of eigenvalues can be explained if the Hessian $\mathbf{H}$ is analyzed as a block diagonal matrix. As pointed out above, in the limit of force constants associated with $\mathbf{q}_s$ approaching infinity, $\mathbf{H}''_{qq}$ becomes diagonal with diagonal elements equal to the diverging force constants, in relation to which all other elements of $\mathbf{H}$ are insignificant. Equation 46 gives a set of $(3N - f)$ eigenvalues that tend to infinity along with the force constants and are obtainable from solving

$$\mathbf{a}^{-1''}\mathbf{H}''_{qq}\mathbf{q}'_s = \lambda\mathbf{q}'_s \qquad (48)$$

The eigenvectors corresponding to these eigenvalues are vibrational modes associated with the stiff degrees of freedom. Lazaridis et al. made similar arguments when considering conformational flips in model proteins.[76]

Appendix B. Calculation of Partition Functions and Jump Rates via a Harmonic Approximation

Each partition function in eq 26 has the general form[103]

$$Q = \frac{1}{h^{3N}\,N_c!}\int \dots \int \mathrm{d}^{3N}P\;\mathrm{d}^{3N}X\;\exp\left(-\frac{H}{k_BT}\right) \qquad (49)$$

Equation 49 represents a system of N_c chains in three dimensions; each of the N/N_c atoms that comprise a chain possess a momentum $\mathbf{P}^i$ and a position $\mathbf{X}^i$, and the total energy H equals the sum of the kinetic energy K and potential energy V. The form of Q is unchanged after switching to mass-weighted Cartesian coordinates, $\mathbf{x}^i \equiv m_i^{1/2}\mathbf{X}^i$, $\mathbf{p}^i \equiv \mathbf{P}^i/m_i^{1/2}$, since the Jacobian of these simultaneous transformations equals unity. The standard[103] analytic integration over the momentum may be performed after substituting for the kinetic energy

$$K = \sum_{i=1}^{N}\frac{|\mathbf{P}^i|^2}{2m_i} = \sum_{i=1}^{N}\frac{1}{2}|\mathbf{p}^i|^2 = \sum_{i=1}^{N}\sum_{\alpha=x,y,z}\frac{1}{2}(p^{i\alpha})^2$$

and assuming velocity-independent forces, yielding

$$Q = \frac{1}{N_c!}\left(\frac{2\pi k_BT}{h^2}\right)^{3N/2}\int \dots \int \mathrm{d}^{3N}x\,\exp(-V/k_BT) \qquad (50)$$

With this step, the flexible model of polymer conformation in the limit of infinite stiffness has been selected, since the uncoupled kinetic energies of all N particles were incorporated. (All thermal modes were activated.) Particle masses remain part of the integrand due to the mass-weighted Cartesian coordinates.

Next, the coordinate system is changed to the generalized coordinates that were used in the polymer simulations.[84] The resulting partition function may be written as

$$Q = \frac{1}{N_c!}\left(\frac{2\pi k_BT}{h^2}\right)^{3N/2}\int \dots \int \mathrm{d}^{3N}q(\det J')\times \exp(-V/k_BT) \qquad (51)$$

where, for N_c polymer chains of n_{un} units and one penetrant molecule, $\mathrm{d}^{3N}q$ and $\det J'$ are defined by[84]

$$\mathrm{d}^{3N}q = \mathrm{d}x_{pen}\,\mathrm{d}y_{pen}\,\mathrm{d}z_{pen}\times \prod_{c=1}^{N_c}\left\{\mathrm{d}x_c^{st}\,\mathrm{d}y_c^{st}\,\mathrm{d}z_c^{st}\,\mathrm{d}\psi_{c1}\,\mathrm{d}\psi_{c2}\,\mathrm{d}\psi_{c3}\left(\prod_{i=1}^{2n_{un}}\mathrm{d}l_{ci}\right)\left(\prod_{i=1}^{n_{un}}\mathrm{d}l_{Rci}\right)\times \left(\prod_{i=1}^{2n_{un}-1}\mathrm{d}\theta_{ci}\right)\left(\prod_{i=1}^{2n_{un}-2}\mathrm{d}\phi_{ci}\right)\left(\prod_{i=1}^{n_{un}}\mathrm{d}\alpha_{ci}\,\mathrm{d}\beta_{ci}\right)\right\} \qquad (52)$$

and

$$\det J' = \prod_{c=1}^{N_c}\left\{\left(\prod_{i=1}^{2n_{un}-1} m_{ci}^{3/2}l_{ci}^{2}\sin\theta_{ci}\right)m_{c,2n_{un}}^{3/2}l_{c,2n_{un}}^{2}\sin\psi_{c2}\times \left(\prod_{i=1}^{n_{un}}\frac{m_{R_{ci}}^{3/2}(-c_i)\,l_{R_{ci}}^{2}\sin\alpha_{ci}\sin\beta_{ci}}{(\sin^2\theta_{ci} - \cos^2\alpha_{ci} - \cos^2\beta_{ci} - 2\cos\alpha_{ci}\cos\beta_{ci}\cos\theta_{ci})^{1/2}}\right)\right\} \qquad (53)$$

The next step is to evaluate this partition function numerically. The harmonic approximation is made in the generalized coordinates in a way such that the results are independent of the coordinate system used; the resulting equations are equivalent to making a harmonic approximation in the mass-weighted Cartesian coordinates. The advantage of harmonic normal modes is that integration over them is analytic (since a harmonic potential leads to a Gaussian integration). However, a representation in terms of flexible generalized coordinates necessitates the incorporation of the covariant and contravariant metric tensors.

The form of the harmonic approximation in mass-weighted Cartesian coordinates is

$$V \approx V_0 + \nabla_{\mathbf{x}}V|_{\mathbf{x}_0}\cdot(\mathbf{x} - \mathbf{x}_0) + \frac{1}{2}(\mathbf{x} - \mathbf{x}_0)^{\mathrm{T}}\mathbf{H}(\mathbf{x} - \mathbf{x}_0) + \dots \qquad (54)$$

The first term is a constant and is independent of the coordinate system. The second term has the same form in generalized coordinates, since transformation would incorporate a product of the matrices J and J' (eqs 10 and 11); their product equals the identity matrix. In any case, this term drops out, since the gradient equals

zero at the local minima and the transition state. Transformation of the third term would incorporate the gradient (via eq 18), but at the local minima and transition state the same form is retained, since the gradient equals zero and an analogous cancelation of Jacobian matrices occurs. Hence,

$$V \approx V_0 + \nabla_{\mathbf{q}} V|_{\mathbf{q}_0} \cdot (\mathbf{q} - \mathbf{q}_0) + \frac{1}{2}(\mathbf{q} - \mathbf{q}_0)^{\mathrm{T}} \mathbf{H}_{qq} (\mathbf{q} - \mathbf{q}_0) + \ldots \quad (55)$$

near either a transition state or a local minimum.

The generalized eigenvalue problem to solve for the normal mode eigenvectors was derived above as eq 23. The modes and their eigenvalues were calculated with a standard matrix package.[104]

The utility of generalized coordinates here was that they are most convenient for defining which coordinates are flexible (i.e., coupled with penetrant jumps) and which are not involved (and therefore kept constant by infinitely stiff springs). However, to perform the harmonic approximation, it is necessary to transform from the generalized coordinates into the normal mode coordinates, defined by the eigenvectors. Any change in configuration may be written as a vector in the f flexible generalized coordinates, $\mathbf{q}_{\mathrm{f}}$; we denote here the change along coordinate i by $(\mathbf{q}_{\mathrm{f}})_i$. We label each eigenvector as $\mathbf{z}_i$, with i distinguishing among the different vector modes. Z_i is the magnitude of the displacement along a particular normal mode i. We denote the vector of all displacements as $\mathbf{Z}$. The eigenvectors span the same space as the flexible coordinates, and the Jacobian of this transformation

$$\mathrm{d}\mathbf{q}_{\mathrm{f}} = |J|\, \mathrm{d}\mathbf{Z}$$

equals the determinant of the matrix $(\partial \mathbf{q}_{\mathrm{f}} / \partial \mathbf{Z})$. To solve for this matrix, recall that two eigenvectors of the generalized eigenvalue problem are orthonormal in the sense that[105]

$$(\mathbf{z}_i)^{\mathrm{T}} \mathbf{a}^0 \mathbf{z}_j = 1 \qquad \text{if } i = j \quad (56)$$

$$= 0 \qquad \text{otherwise}$$

Writing the eigenvectors $\mathbf{z}_i$ as columns of a matrix $\mathbf{S}$,

$$\mathbf{S} = \begin{pmatrix} | & | & & | \\ \mathbf{z}_1 & \mathbf{z}_2 & \ldots & \mathbf{z}_f \\ | & | & & | \end{pmatrix}$$

orthonormality may be summarized as

$$\mathbf{S}^{\mathrm{T}} \mathbf{a}^0 \mathbf{S} = I \quad (57)$$

By definition, the motions along an eigenvector $\mathbf{z}_i$ may be interpreted as

$$\mathbf{z}_i = \begin{pmatrix} \text{motion} & \text{along} & q_1 & \text{in} & \text{normal} & \text{mode} & i & \text{for} & \text{unit} & \text{displacement} & Z_i = 1 \\ " & " & q_2 & " & " & " & i & " & " & " & " \\ " & " & q_3 & " & " & " & i & " & " & " & " \\ \vdots & \vdots & \vdots & \vdots & \vdots & \vdots & \vdots & \vdots & \vdots & \vdots & \vdots \\ " & " & q_f & " & " & " & i & " & " & " & " \end{pmatrix}$$

since a step along the $\mathbf{z}_i$ direction changes the generalized coordinate q_j by the amount $(\mathbf{z}_i)_j$. Mathematically, this implies that the derivative

$$\frac{\partial q_j}{\partial Z_i} = (\mathbf{z}_i)_j$$

Collecting the different coordinates in a column,

$$\frac{\partial \mathbf{q}_{\mathrm{f}}}{\partial Z_i} = \mathbf{z}_i = \begin{pmatrix} | \\ \mathbf{z}_i \\ | \end{pmatrix} \quad (58)$$

where the last term indicates that $\mathbf{z}_i$ is a column vector. Arranging the derivatives with respect to different normal modes along different columns leads to

$$\frac{\partial \mathbf{q}}{\partial \mathbf{Z}} = \begin{pmatrix} | & | & & | \\ \mathbf{z}_1 & \mathbf{z}_2 & \ldots & \mathbf{z}_f \\ | & | & & | \end{pmatrix} \quad (59)$$

and consequently the Jacobian $|J| = |\partial \mathbf{q}_{\mathrm{f}} / \partial \mathbf{Z}|$ equals the determinant of $\mathbf{S}$. From eq 57, $\det(\mathbf{S}^{\mathrm{T}} \mathbf{a}^0 \mathbf{S}) = \det \mathbf{S}^{\mathrm{T}} \det \mathbf{a}^0 \det \mathbf{S} = \det I$, or

$$|J| = \det \mathbf{S} = \sqrt{1/\det \mathbf{a}^0} \quad (60)$$

and

$$\mathrm{d}\mathbf{q}_{\mathrm{f}} = \sqrt{\frac{1}{\det \mathbf{a}^0}}\, \mathrm{d}\mathbf{Z} \quad (61)$$

The partition function

$$Q = \frac{1}{N_{\mathrm{c}}!} \left(\frac{2\pi k_{\mathrm{B}} T}{h^2} \right)^{3N/2} \int \ldots \int \mathrm{d}^f Z\, \mathrm{d}^{3N-f} q_{\mathrm{s}}' \, (\det J') \times \sqrt{\frac{1}{\det \mathbf{a}^0}} \exp(-V/k_{\mathrm{B}} T)$$

now contains normal modes of the flexible generalized coordinates, at the cost of introducing another Jacobian factor.

The remaining step is the transformation of the infinitely stiff generalized coordinates into their corresponding normal modes. From the Fixman relation,[90,106]

$$\det \mathbf{a} \det \mathbf{a}^{-1''} = \det \mathbf{a}^0 \quad (62)$$

the Jacobian factors will cancel if normal modes can be chosen such that the Jacobian of this transformation equals $\sqrt{1/\det \mathbf{a}^{-1''}}$. As discussed in Appendix A following eq 46, the corresponding generalized eigenvalue problem to solve is

$$\mathbf{H}_{q'q'} \mathbf{z}' = \lambda' \left[\left(\mathbf{a}^{-1''} \right)^{-1} \right] \mathbf{z}' \quad (63)$$

for the normal modes $\mathbf{z}'$ that span the same space as the infinitely stiff generalized coordinates. The change from infinitely stiff generalized coordinates to their corresponding normal modes results in a Jacobian, $|J| = \sqrt{1/\det(\mathbf{a}^{-1''})^{-1}}$, that is analogous to that of the

flexible coordinates and thus leads to an expression for the partition function

$$Q = \frac{1}{N_c!}\left(\frac{2\pi k_B T}{h^2}\right)^{3N/2} \int \dots \int d\mathbf{Z}\, d\mathbf{Z}' \times (\det J')\sqrt{\frac{\det \mathbf{a}^{-1''}}{\det \mathbf{a}^0}} \exp(-V/k_B T) \quad (64)$$

where $\mathbf{Z}'$ is a $(3N - f)$-dimensional vector that represents the magnitudes of the normal modes that arose from the infinitely stiff degrees of freedom. In the normal-mode coordinate system, the approximate potential energy of eq 54 takes the form

$$V \approx V_0 + \sum_{\alpha=1}^{f} \lambda_\alpha Z_\alpha^2 + \sum_{A=1}^{3N-f} \lambda'_A Z'^2_A + \dots \quad (65)$$

since the Hessian matrix is diagonal in this coordinate system. Noting that det $\mathbf{a} = (\det J')^2$ and using the Fixman relation, the determinants cancel, leaving a set of $3N$ independent integrals.

Each integral

$$\int dZ_i \exp\left(-\frac{\lambda_i Z_i^2}{2k_B T}\right) = \sqrt{\frac{2\pi k_B T}{\lambda_i}}$$

may be evaluated for the flexible modes, since the frequencies are finite. Combined with the prefactors from the kinetic energy, the classical vibrational partition function for each flexible normal mode i can be written

$$q^{CL}_{vib\ i} = \frac{k_B T}{h\nu_i} \quad (66)$$

with the frequency ν_i defined by eq 24.

For the infinitely stiff normal modes, each frequency approaches infinity, and the individual classical vibrational partition functions cannot be considered; each one would approach zero, since $\nu_i = 1/2\pi\sqrt{k_{stiff}/m} \rightarrow \infty$. However, the products of these $3N - f$ terms may be compared at the transition state and at the associated local minima by the following argument. Recall the eigenvalue problem that must be solved (conceptually, not numerically) for the eigenvalues of the infinitely stiff normal modes, eq 63. If one multiplies by the inverse of the metric tensor, eq 63 becomes

$$(\mathbf{a}^{-1''})\mathbf{H}_{q'q'}\mathbf{z}' = \lambda'\mathbf{z}'$$

One way to obtain the eigenvalues would be to move the eigenvalue−eigenvector product to the left-hand side,

$$\left[(\mathbf{a}^{-1''})\mathbf{H}_{q'q'} - \lambda' I\right]\mathbf{z}' = 0 \quad (67)$$

This equation has a real solution only if the matrix difference is singular (its determinant equals zero). Since that condition is satisfied at only the particular eigenvalues λ'_i, the determinant can be set equal to a characteristic polynomial,

$$\det[\mathbf{a}^{-1''}\mathbf{H}_{q'q'} - \lambda' I] = \prod_{i=1}^{3N-f} (\lambda'_i - \lambda') \quad (68)$$

which has roots at the eigenvalues $\lambda' = \lambda'_i$. If the value of λ' is then set to zero, the resulting equation

$$\det\left[\mathbf{a}^{-1''}\mathbf{H}_{q'q'}\right] = \prod_{i=1}^{3N-f} \lambda'_i \quad (69)$$

yields the product of the eigenvalues (and hence of the frequencies) in terms of determinants of the metric tensor of the stiff coordinates, which is conformation dependent, and the Hessian with respect to the stiff coordinates, which depends only on the force constants that approach infinity. The metric tensor determinant can be evaluated via the Fixman relation (eq 62), with det $\mathbf{a}^0$ and det $\mathbf{a}$ calculated directly.[84] For systems in which all bond and torsion angles are flexible simultaneously, a recursion relation valid for chains with pendant groups has been developed and presented elsewhere.[84]

Combining the vibrational partition functions for individual normal modes, the partition function for a local minimum state may be written classically as

$$Q^{CL} = \frac{1}{N_c!}\prod_{\alpha=1}^{f}\frac{k_B T}{h\nu_\alpha}\prod_{A=1}^{3N-f}\frac{k_B T}{h\nu'_A}\exp(-V_0/k_B T)$$

$$= \frac{1}{N_c!}\prod_{\alpha=1}^{f}\frac{k_B T}{h\nu_\alpha}\left(\frac{k_B T}{h}\right)^{3N-f}\left[\frac{(4\pi^2)^{3N-f}}{\det \mathbf{a}^{-1''}\det \mathbf{H}_{q'q'}}\right]^{1/2} \times \exp(-V_0/k_B T) \quad (70)$$

with det $\mathbf{a}^{-1''}$ evaluated in the local-minimum conformation.

The partition function of the transition state region has a similar form. Since the dividing surface is approximated as a hyperplane, the transition state region is defined by

$$-\infty < Z_i < \infty \quad i \neq 1$$

$$Z_i = 0 \quad i = 1$$

Consequently, only the modes with real frequencies (positive eigenvalues) are integrated over. The resulting expression for the transition state region partition function is

$$Q^{\ddagger\,CL} = \frac{1}{N_c!}\prod_{\alpha=2}^{f}\frac{k_B T}{h\nu^{\ddagger}_\alpha}\left(\frac{k_B T}{h}\right)^{3N-f}\left[\frac{(4\pi^2)^{3N-f}}{\det (\mathbf{a}^{-1''})^{\ddagger}\det \mathbf{H}_{q'q'}}\right]^{1/2}\exp(-V^{\ddagger}/k_B T) \quad (71)$$

and the superscript ‡ indicates that the frequencies, metric tensor, and partition function have been evaluated at the transition state.

An equation for the penetrant jump rate constant may now be formed by combining eq 26 with eqs 70 and 71. Combining the classical partition functions, the $k_B T/h$ factors and the model-dependent det $\mathbf{H}_{q'q'}$ cancel, yielding eq 28 for the rate constant. The stiff−stiff submatrix of the Hessian is the same at the transition state and the local minima in the limit of infinite stiffness, since it is dominated by the diagonal terms k_{stiff}. Hence the rate depends solely on the ratio of frequencies, the

ratio of $\mathbf{a}^{-1''}$ at the two locations, and the energy difference between states.

A different method for treating the classical vibrational partition function (i.e., its approach to zero at large, finite frequencies) was suggested by Gilbert.[107] We replace (conceptually) the classical Hamiltonian in the normal-mode coordinates with an equivalent, quantum-mechanical one. The resulting vibrational partition function

$$q_{\mathrm{vib}_i}^{\mathrm{QM}} = \left[1 - \exp\left(-\frac{h\nu_i}{k_{\mathrm{B}}T}\right)\right]^{-1}$$

becomes unity at high frequencies and equals the classical expression, eq 66, at low frequencies. The zero-point energy has been neglected equally in all modes. The distinction among eigenvalues that approach infinity (corresponding to the normal modes of infinitely stiff generalized coordinates) vanishes in this limit, since all the associated vibrational partition functions become unity. The resulting partition function for a local-minimum state can be written quantum-mechanically as

$$\begin{aligned} Q^{\mathrm{QM}} &= \frac{1}{N_c!}\prod_{\alpha=1}^{f}\left[1 - \exp\left(-\frac{h\nu_\alpha}{k_{\mathrm{B}}T}\right)\right]^{-1} \times \\ &\qquad \prod_{A=1}^{3N-f}\lim_{\nu_A\to\infty}\left[1 - \exp\left(-\frac{h\nu_A}{k_{\mathrm{B}}T}\right)\right]^{-1} \exp(-V_0/k_{\mathrm{B}}T) \\ &= \frac{1}{N_c!}\prod_{\alpha=1}^{f}\left[1 - \exp\left(-\frac{h\nu_\alpha}{k_{\mathrm{B}}T}\right)\right]^{-1} \exp(-V_0/k_{\mathrm{B}}T) \quad (72) \end{aligned}$$

The conformation dependence of the stiff modes vanishes in the limit of infinite stiffness. The partition function for the transition state region is analogous (compare eqs 70 and 71). Combining the quantum-mechanical partition functions leads to the rate constant of eq 29.

References and Notes

(1) Meares, P. *J. Am. Chem. Soc.* **1954**, *76*, 3415−3422.
(2) Brandt, W. W. *J. Phys. Chem.* **1959**, *63*, 1080−1084.
(3) DiBenedetto, A. T. *J. Polym. Sci.* **1963**, *A1*, 3477−3487.
(4) Pace, R. J.; Datyner, A. *J. Polym. Sci., Polym. Phys. Ed.* **1979**, *17*, 437−451.
(5) Pace, R. J.; Datyner, A. *J. Polym. Sci., Polym. Phys. Ed.* **1979**, *17*, 453−464.
(6) Pace, R. J.; Datyner, A. *J. Polym. Sci., Polym. Phys. Ed.* **1979**, *17*, 465−476.
(7) Fujita, H. *Fortschr. Hochpolym.-Forsch.* **1961**, *3*, 1−47.
(8) Vrentas, J. S.; Duda, J. L. *J. Polym. Sci., Polym. Phys. Ed.* **1977**, *15*, 403−416.
(9) Vrentas, J. S.; Duda, J. L. *J. Polym. Sci., Polym. Phys. Ed.* **1977**, *15*, 417−439.
(10) Vrentas, J. S.; Duda, J. L. *J. Polym. Sci., Polym. Phys. Ed.* **1977**, *15*, 441−453.
(11) Zielinski, J. M.; Duda, J. L. *AIChE J.* **1992**, *38*, 405−415.
(12) Petropoulos, J. H. *J. Polym. Sci., Polym. Phys. Ed.* **1970**, *8*, 1797−1801.
(13) Paul, D. R.; Koros, W. J. *J. Polym. Sci., Polym. Phys. Ed.* **1976**, *14*, 675−685.
(14) Fredrickson, G. H.; Helfand, E. *Macromolecules* **1985**, *18*, 2201−2207.
(15) Vieth, W. R. *Diffusion in and through Polymers: Principles and Applications*; Hansen: New York, 1991.
(16) Neogi, P. *Diffusion in Polymers*; Marcel Dekker: New York, 1996.
(17) Greenfield, M. L.; Theodorou, D. N. *Mol. Simul.* **1997**, *19*, 329−361.
(18) Trohalaki, S.; Rigby, D.; Kloczkowski, A.; Mark, J. E.; Roe, R.-J. *Polym. Prepr. (Am. Chem. Soc., Div. Polym. Chem.)* **1989**, *30* (2), 23−24.
(19) Takeuchi, H. *J. Chem. Phys.* **1990**, *93*, 2062−2067.
(20) Takeuchi, H.; Roe, R.-J.; Mark, J. E. *J. Chem. Phys.* **1990**, *93*, 9042−9048.
(21) Takeuchi, H.; Okazaki, K. *J. Chem. Phys.* **1990**, *92*, 5643−5652.
(22) Takeuchi, H. *J. Chem. Phys.* **1990**, *93*, 4490−4491.
(23) Müller-Plathe, F. *J. Chem. Phys.* **1991**, *94*, 3192−3199.
(24) Takeuchi, H.; Okazaki, K. *Makromol. Chem., Macromol. Symp.* **1993**, *65*, 81−88.
(25) Boyd, R. H.; Pant, P. V. K. *Macromolecules* **1991**, *24*, 6325−6331.
(26) Pant, P. V. K.; Boyd, R. H. *Macromolecules* **1993**, *26*, 679−686.
(27) Sonnenburg, J.; Gao, J.; Weiner, J. H. *Macromolecules* **1990**, *23*, 4653−4657.
(28) Müller-Plathe, F. *J. Chem. Phys.* **1992**, *96*, 3200−3205.
(29) Müller-Plathe, F.; Rogers, S. C.; van Gunsteren, W. F. *Macromolecules* **1992**, *25*, 6722−6724.
(30) Müller-Plathe, F.; Rogers, S. C.; van Gunsteren, W. F. *Chem. Phys. Lett.* **1992**, *199*, 237−243.
(31) Tamai, Y.; Tanaka, H.; Nakanishi, K. *Macromolecules* **1994**, *27*, 4498−4508.
(32) Han, J.; Boyd, R. H. *Macromolecules* **1994**, *27*, 5365−5370.
(33) Takeuchi, H.; Okazaki, K. *Mol. Simul.* **1996**, *16*, 59−74.
(34) Chassapis, C. S.; Petrou, J. K.; Petropoulos, J. H.; Theodorou, D. N. *Macromolecules* **1996**, *29*, 3615−3624.
(35) Fukuda, M.; Kuwajima, S. *J. Chem. Phys.* **1997**, *107*, 2149−2158.
(36) Sok, R. M.; Berendsen, H. J. C.; van Gunsteren, W. F. *J. Chem. Phys.* **1992**, *96*, 4699−4704.
(37) Li, T.; Kildsig, D. O.; Park, K. *J. Control. Release* **1997**, *48*, 57−66.
(38) Gee, R. H.; Boyd, R. H. *Polymer* **1995**, *36*, 1435−1440.
(39) Gusev, A. A.; Müller-Plathe, F.; van Gunsteren, W. F.; Suter, U. W. *Adv. Polym. Sci.* **1994**, *116*, 207−247.
(40) Smit, E.; Mulder, M. H. V.; Smolders, C. A.; Karrenbeld, H.; van Eerden, J.; Feil, D. *J. Membr. Sci.* **1992**, *73*, 247−257.
(41) Zhang, R.; Mattice, W. L. *J. Membr. Sci.* **1995**, *108*, 15−23.
(42) Han, J.; Boyd, R. H. *Polymer* **1996**, *37*, 1797−1804.
(43) Bassolino-Klimas, D.; Alper, H. E.; Stouch, T. R. *Biochemistry* **1993**, *32*, 12624−12637.
(44) Bassolino-Klimas, D.; Alper, H. E.; Stouch, T. R. *J. Am. Chem. Soc.* **1995**, *117*, 4118−4129.
(45) Berendsen, H. J. C.; Marrink, S.-J. *Pure Appl. Chem.* **1993**, *65*, 2513−2520.
(46) Marrink, S.-J.; Berendsen, H. J. C. *J. Phys. Chem.* **1994**, *98*, 4155−4168.
(47) Alper, H. E.; Stouch, T. R. *J. Phys. Chem.* **1995**, *99*, 5724−5731.
(48) Theodorou, D. N. In *Diffusion in Polymers*; Neogi, P., Ed.; Marcel Dekker: New York, 1996; pp 67−142.
(49) Pant, P. V. K.; Boyd, R. H. *Macromolecules* **1992**, *25*, 494−495.
(50) Müller-Plathe, F.; Laaksonen, L.; van Gunsteren, W. F. *J. Mol. Graphics* **1993**, *11*, 118−120, 125−126.
(51) Greenfield, M. L.; Theodorou, D. N. *Macromolecules* **1993**, *26*, 5461−5472.
(52) Müller-Plathe, F.; Rogers, S. C.; van Gunsteren, W. F. *J. Chem. Phys.* **1993**, *98*, 9895−9904.
(53) Sunderrajan, S.; Hall, C. K.; Freeman, B. D. *J. Chem. Phys.* **1996**, *105*, 1621−1632.
(54) The rate constant calculated by TST places an upper bound on the true rate, since it is assumed that all trajectories that cross the dividing surface terminate in the product state.[55]
(55) Steinfeld, J. I.; Francisco, J. S.; Hase, W. L. *Chemical Kinetics and Dynamics*; Prentice-Hall: Englewood Cliffs, NJ, 1989.
(56) Jagodic, F.; Borstnik, B.; Azman, A. *Makromol. Chem.* **1973**, *173*, 221−231.
(57) Arizzi, S. Diffusion of Small Molecules in Polymeric Glasses: A Modelling Approach. Ph.D. Thesis, MIT, 1990.
(58) Gusev, A. A.; Arizzi, S.; Suter, U. W.; Moll, D. J. *J. Chem. Phys.* **1993**, *99*, 2221−2227.
(59) Gusev, A. A.; Suter, U. W. *J. Chem. Phys.* **1993**, *99*, 2228−2234.
(60) Gusev, A. A.; Suter, U. W.; Moll, D. J. *Macromolecules* **1995**, *28*, 2582−2584.
(61) Gray-Weale, A. A.; Henchman, R. H.; Gilbert, R. G.; Greenfield, M. L.; Theodorou, D. N. *Macromolecules* **1997**, *30*, 7296−7306.

(62) Cerjan, C. J.; Miller, W. H. *J. Chem. Phys.* **1981**, *75*, 2800−2806.
(63) Baker, J. *J. Comput. Chem.* **1986**, *7*, 385−395.
(64) Fukui, K. *Acc. Chem. Res.* **1981**, *14*, 363−368.
(65) Page, M.; McIver, J. W., Jr. *J. Chem. Phys.* **1987**, *88*, 922−935.
(66) Gonzalez, C.; Schlegel, H. B. *J. Phys. Chem.* **1990**, *94*, 5523−5527.
(67) Fischer, S.; Karplus, M. *Chem. Phys. Lett.* **1992**, *194*, 252−261.
(68) Schlegel, H. B. *Adv. Chem. Phys.* **1987**, *67*, 249−286.
(69) Pratt, L. R. *J. Chem. Phys.* **1986**, *85*, 5045−5048.
(70) Czerminski, R.; Elber, R. *Int. J. Quantum Chem.* **1990**, *24*, 167−186.
(71) Gillilan, R.; Wilson, K. R. *J. Chem. Phys.* **1992**, *97*, 1757−1772.
(72) Sevick, E. M.; Bell, A. T.; Theodorou, D. N. *J. Chem. Phys.* **1993**, *98*, 3196−3212.
(73) Schenter, G.; Mills, G.; Jōnsson, H. *J. Chem. Phys.* **1994**, *101*, 8964−8971.
(74) Zimmer, M. F. *Phys. Rev. Lett.* **1995**, *75*, 1431−1434.
(75) Bulatov, V. V.; Argon, A. S. *Phys. Rev. A* **1992**, *46*, 5275−5278.
(76) Lazaridis, T.; Tobias, D. J.; Brooks, C. L.; Paulaitis, M. E. *J. Chem. Phys.* **1991**, *95*, 7612−7625.
(77) Khare, R.; Paulaitis, M. E. *Chem. Eng. Sci.* **1994**, *49*, 2867−2879.
(78) Khare, R.; Paulaitis, M. E. *Macromolecules* **1995**, *28*, 4495−4504.
(79) van Kampen, N. G. *Stochastic Processes in Physics and Chemistry*, revised edition; North-Holland: Amsterdam, 1992.
(80) Theodorou, D. N.; Suter, U. W. *Macromolecules* **1985**, *18*, 1467−1478.
(81) Hansen, J. P.; McDonald, I. R. *Theory of Simple Liquids*; Academic Press: New York, 1976.
(82) Fleming, G. K.; Koros, W. J. *Macromolecules* **1986**, *19*, 2285−2291.
(83) Mansfield, K. F.; Theodorou, D. N. *Macromolecules* **1991**, *24*, 6283−6294.
(84) Greenfield, M. L. Molecular Modeling of Dilute Penetrant Gas Diffusion in a Glassy Polymer using Multidimensional Transition State Theory. Ph.D. Thesis, University of California at Berkeley, 1996.
(85) Weiner, J. H. *Statistical Mechanics of Elasticity*; Wiley-Interscience: New York, 1983.
(86) This usage of "steepest descent" refers to a path constructed by taking a sequence of small steps, each directed opposite to the local gradient. This usage differs from that in the optimization literature; there,[87] the magnitude of each step is chosen such that the objective function is minimized with respect to motion along the step vector.
(87) Press: W. H.; Flannery, B. P.; Teukolsky, S. A.; Vetterling, W. T. *Numerical Recipes, The Art of Scientific Computing*; Cambridge University Press: Cambridge, 1989.
(88) Banerjee, A.; Adams, N. P. *Int. J. Quantum Chem.* **1992**, *43*, 855−871.
(89) Pechukas, P. *J. Chem. Phys.* **1976**, *64*, 1516−1521.
(90) Gō, N.; Scheraga, H. A. *Macromolecules* **1976**, *9*, 535−542.
(91) Vineyard, G. H. *J. Phys. Chem. Solids* **1957**, *3*, 121−127.
(92) Zemke, K.; Chmelka, B. F.; Schmidt-Rohr, K.; Spiess, H. W. *Macromolecules* **1991**, *24*, 6874−6876.
(93) van Gunsteren, W. F.; Karplus, M. *Macromolecules* **1982**, *15*, 1528−1544.
(94) In some circumstances, the conformation resulting from the transition state search that satisfied condition 1 would have new segments within the cutoff distance, implying additional generalized coordinates to release. Condition 2 would be false in such a case. A search would be conducted in this newly augmented set of generalized coordinates, with the resulting transition state structure again subject to both conditions.
(95) Dongarra, J. J.; Bunch, J. R.; Moler, C. B.; Stewart, G. W. *LINPACK User's Guide*; SIAM: Philadelphia, 1979.
(96) Seeley, G.; Keyes, T. *J. Chem. Phys.* **1989**, *91*, 5581−5586.
(97) Keyes, T. *J. Chem. Phys.* **1994**, *101*, 5081−5092.
(98) Straub, J. E.; Thirumalai, D. *Proc. Natl. Acad. Sci. U.S.A.* **1993**, *90*, 809−813.
(99) Zwanzig, R. *Proc. Natl. Acad. Sci. U.S.A.* **1988**, *85*, 2029−2030.
(100) Bassler, H. *Phys. Rev. Lett.* **1987**, *58*, 767−770.
(101) Starkweather, H. W. *Polymer* **1991**, *32*, 2443−2448.
(102) Chandrasekhar, S. *Rev. Mod. Phys.* **1943**, *15*, 1−89.
(103) Hill, T. L. *An Introduction to Statistical Thermodynamics*; Addison-Wesley: Reading, MA, 1962. Reprint published by Dover Publications: Mineola, NY, 1986.
(104) Smith, B. T.; Boyle, J. M.; Garbow, B. S.; Ikebe, Y.; Klema, V. C.; Moler, C. B. *Matrix Eigensystem Routines: EISPACK guide*, 2nd ed.; Springer-Verlag: New York, 1976.
(105) Strang, G. *Linear Algebra and its Applications*; Academic Press: Orlando, FL, 1980.
(106) Fixman, M. *Proc. Natl. Acad. Sci. U.S.A.* **1974**, *71*, 3050−3053.
(107) Gilbert, R. G. Personal communication, June 1995.

MA980750H